The bromodomain inhibitor JQ1 is a molecular glue targeting centromeres.

Samuel Corless[1,2], Noor Pratap-Singh[3], Nezha S. Benabdallah[4], Jasmin Böhm[1], Alexander M. Simon[1,2], Vojtěch Dolejš[1,2], Simon Anders[2], Ana Banito[4] and Sylvia Erhardt[1,2]*

[1]Karlsruhe Institute of Technology (KIT) - South Campus, Zoological Institute, Molecular Cell Biology, Fritz-Haber-Weg 4, D-76131 Karlsruhe, Germany

[2]University of Heidelberg, Center for Molecular Biology Heidelberg (ZMBH), Im Neuenheimer Feld 282, 69120 Heidelberg, Germany

[3]University of Maryland, Department of Computer Science, College Park, MD 20740, USA

[4]German Cancer Research Center (DKFZ), Soft-Tissue Sarcoma (B380), Im Neuenheimer Feld 581, 69120 Heidelberg, Germany

*Correspondence to: sylvia.erhardt@KIT.edu

One sentence summary

The inhibitor JQ1 links BRD4 and CENP-B as a molecular glue and reveals a function in centromere cohesion and JQ1 resistance

Abstract

Centromeres are essential for cell proliferation and a promising target for anti-cancer therapies, yet no drugs have been identified that specifically target centromeric chromatin. To identify candidates, we analysed chromatin proteins at repetitive loci using a novel big-data approach and discovered the bromodomain protein BRD4 localises to centromeres, a localisation enhanced by the bromodomain inhibitor JQ1. While bromodomain inhibitors typically prevent BRD4 from binding chromatin, we found that JQ1 stabilises an interaction between BRD4 and the centromere protein CENP-B. Degradation of BRD4 caused centromere cohesion defects, whereas JQ1-treatment preserved centromere structure in a CENP-B dependent manner. Strikingly, JQ1-resistant cells became reliant on CENP-B for proliferation. Our results identify a non-canonical role for BRD4 in centromere cohesion and establish JQ1 as a molecular-glue targeting centromeric chromatin.

30 **Introduction**

31 Human centromeres have long been considered an enigmatic and challenging region of the
32 genome to study using sequencing-based approaches, due to the highly repetitive nature of their
33 DNA (Fig. 1a)[1]. The function of centromeric loci is to ensure the accurate partitioning of the
34 genome during cell-division by assembling the multi-subunit kinetochore complex, which
35 attaches chromosomes to the spindle microtubules in mitosis[2,3]. Defects in centromere structure
36 and function are key drivers of aneuploidy, tumour heterogeneity and cancer progression[4,5].
37 Furthermore, the centromere-dependent spindle assembly checkpoint, which prevents
38 catastrophic chromosome segregation errors, is often the last checkpoint preserved in aneuploid
39 cells which makes many cancers exceptionally sensitive to inhibitors of mitotic components[6,7].
40 Such diverse roles indicate that centromeric proteins are an attractive target for anti-cancer
41 therapeutics, but there are no known drugs that specifically target components of centromeric
42 chromatin. A major barrier to progress in human centromere biology has been the lack of
43 studies mapping chromatin proteins to highly-repetitive DNA regions[8], and for the most-part
44 our understanding of centromeric chromatin remains in the pre-genomic era.

45 In contrast to centromeres, our understanding of chromatin within unique-sequence regions has
46 been revolutionised thanks to the wide-scale application of genome-wide chromatin mapping
47 approaches, which have significantly improved our understanding of the molecular
48 mechanisms of transcription factors[9], regulatory elements[10], 3D genome organisation[11],
49 chromatin-associated disease[12,13] and specific classes of small-molecule inhibitors targeting
50 chromatin components[12]. In these published studies centromeric loci were excluded from the
51 analysis, either through the use of a genome-build in which centromeric repeats are absent or
52 because standard pipelines exclude repetitive DNA[1], but the raw experimental data containing
53 this information is publicly accessible through the Sequence Read Archive (SRA)[14]. We took
54 advantage of this vast resource and developed an approach that utilises published chromatin-
55 mapping datasets to identify the protein composition of any locus, with a focus on centromeric
56 chromatin. Utilising tens-of-thousands of samples we were able to identify established and
57 novel proteins associated with different loci-of-interest. We then characterised a sub-set of this
58 data in which drug-treatments were performed, aiming to identify drugs that affect the protein
59 composition of centromeres.

60 In this study we identify an unexpected enrichment of the BET bromodomain protein BRD4[15]
61 at centromeres and demonstrate a new function for this protein in the regulation of centromeric

62 cohesion[16]. We then demonstrate that the BET bromodomain inhibitor JQ1[17] further recruits
63 BRD4 to the centromere, in contrast to its canonical mechanism antagonising the association
64 of BRD4 with chromatin[18]. We show that JQ1 stabilises a protein-protein interaction between
65 BRD4 and the centromere DNA binding protein CENP-B[19], identifying the first case of a drug
66 directly targeting centromeric chromatin. Drugs that stabilise protein-protein interactions,
67 called molecular-glues, often accentuate one particular function of a protein[20,21]. CENP-B
68 removal reveals that JQ1 treatment stabilises centromere cohesion, demonstrating a direct
69 effect of the BRD4-JQ1-CENP-B interaction on centromeric cohesion. Finally, we observe in
70 a pre-clinical model of JQ1-resistance that CENP-B transitions from non-essential in parental
71 cells to the most significant determinant of cell-proliferation in JQ1-resistant cells, suggesting
72 that our newly discovered mechanism-of-action has important clinical implications.

73

74 ***REDPOINT reveals the presence of BRD4 at centromeric chromatin***

75 To identify chromatin proteins at specific loci, and how they change upon various drug
76 treatments, we developed an approach called Reanalysis of Every Dataset at Positions Of
77 INTerest (REDPOINT). Our analysis includes 40,733 chromatin immunoprecipitation
78 sequencing (ChIP-seq) experiments that identify the genomic distribution of more than 1200
79 human chromatin proteins and post-translational modifications (Fig. 1b). The workflow
80 included the following steps: 1) download 100,000 reads per ChIP-seq sample from the SRA,
81 2) align to a human genome build which includes information for repetitive loci[1], 3) retain
82 repetitive regions and identify the percentage of reads at each locus of interest compared to the
83 whole genome, 4) repeat for each dataset, 5) annotate and analyse the data. As a proof-of-
84 principle we considered a selection of biologically interesting sequences, including different
85 repetitive regions (e.g. centromeres, rDNA), selected Topological Associated Domain (TAD)
86 boundaries and gene promoters. The top hits for selected loci contain well-characterized locus-
87 specific proteins and proteins that have only recently been identified in association with
88 specific loci, such as NIPBL and RNA polymerase II for rDNA[22,23], and GTF2I and BRD4 for
89 TAD boundaries[24,25] (Fig. 1c and 1d). This shows that REDPOINT accurately characterizes the
90 chromatin composition at DNA sequences varying from 500 bp to 60 Mbp, e.g. over five orders
91 of magnitude. Most importantly, we identify new candidate proteins at each locus.

92 Focusing on centromeric DNA we observe a striking enrichment of proteins previously
93 identified at the centromere-core which is the site of kinetochore formation and microtubule

94 attachment during chromosome segregation[26] (CENP-A, CENP-B, CENP-C, CENP-T),
95 pericentromeric heterochromatin which supports centromere-core function[27] (HP1α, HP1β,
96 DNMT1, DNMT3A, ATRX) and other proteins with centromeric roles (LRWD1, TRF2,
97 DDX11, TOP2α, HIRA, RAC3, SMAD3, BCL6) (Fig. 1a and 1d). We also identified 19 high
98 confidence new centromere protein candidates, which met one or both of the following criteria:
99 1) more than two-fold enriched compared to corresponding control, 2) in the top 500 samples
100 by percent of reads aligned to the centromere. Within the new centromere candidates was
101 BRD4, a key protein in the organization of super-enhancers, transcription elongation and
102 interphase genome organization[15,25,28].

103 Next, we aimed to discover one or more drugs that specifically target centromeric chromatin.
104 REDPOINT contains ChIP-seq samples for proteins in cells treated with 96 different small-
105 molecule compounds, including 50 protein-drug pairs investigated across multiple studies.
106 Focussing on this subset, we identify that BRD4-JQ1 stands out as the only protein-drug
107 combination that highly significantly changes protein abundance at the centromere across
108 different studies (Fig. 1e). JQ1 is a small-molecule BET bromodomain inhibitor that prevents
109 BRD4 from binding its acetyl-chromatin substrate[18], so the canonical mechanism-of-action
110 would predict that JQ1-treatment decreases BRD4 levels at its chromatin binding sites.
111 Unexpectedly, we observe that JQ1 treatment consistently increases BRD4 occupancy at
112 centromeric loci across multiple studies.

113 The discovery of the presence and drug-induced increase of BRD4 at centromeres is
114 remarkable. Typically, BRD4 is considered as a regulator of genes and enhancers[15], but
115 centromeric regions lack these elements and are mostly transcriptionally inactive[8,29]. Recent
116 studies have revealed that BRD4 also plays a role in the organisation of the interphase genome
117 by promoting cohesin loading at TAD boundaries, indicating a role in contemporary theories
118 of genome organisation through chromatin loop extrusion. However, the cohesin complex was
119 originally characterised with respect to its role in centromere structure, where it maintains sister
120 chromatid cohesion to regulate accurate chromosome segregation. While prior studies have not
121 suggested a role for BRD4 in centromeric cohesion, our observations have led us to investigate
122 the role of BRD4 and the inhibitor JQ1 at centromeric loci.

123

124 ***BRD4 plays a non-canonical role in centromere chromatid cohesion***

125 To confirm that BRD4 is specifically enriched at centromeres we took advantage of a recently
126 released Telomere-to-Telomere (T2T) genome build which, by using long reads sequencing,
127 identified the precise linear mapping of the genome including megabase-sized regions of highly
128 repetitive DNA at centromeres[8,30]. Aligning ChIP-seq samples from diverse cell types we
129 observed BRD4 at many sites along the chromosome, including at centromeric loci defined by
130 the co-localisation with CENP-A and HP1 (Fig. 2a).

131 To identify the specific chromatin sub-domain that BRD4 associates with within centromeric
132 DNA, we performed immunofluorescence in HeLa cells with antibodies targeting BRD4 and
133 CENP-A (Fig. 2b). The overall distribution of BRD4 was consistent with previous studies,
134 being highly enriched in euchromatin regions with low DAPI density and mostly excluded
135 from DAPI-dense heterochromatin at the periphery of the nucleus and nucleoli[31]. Focusing on
136 the core-centromere, we observe a clear co-localisation between BRD4 and CENP-A. Within
137 the heterochromatin surrounding nucleoli CENP-A and BRD4 are enriched together at clear
138 puncta, demonstrating that BRD4 is confined to the core-centromere and is absent from the
139 surrounding pericentromeric heterochromatin. This observation confirms that BRD4 is a
140 centromere protein that localises to the centromere-core region.

141 The canonical role of BRD4 is to bind acetylated chromatin and recruit the transcription
142 machinery[15], but centromeres have well-characterised depletions of acetylated chromatin and
143 are considered the archetypal locus for transcriptionally repressed heterochromatin[27,32]. We
144 confirmed that centromeric BRD4 enrichment does not correspond to an enrichment in
145 H3K27ac or RNA polymerase II at the centromere (Fig. 2a and 2c), indicating that BRD4 may
146 act through a non-canonical mechanism.

147 Recent work has identified a non-canonical role for BRD4 upstream of cohesin loading[25,33,34].
148 To investigate this role, we first set out to completely deplete BRD4 from cells, including
149 centromeres. We utilised MZ1, a proteolysis-targeted chimera (PROTAC) small molecule that
150 selectively degrades BRD4 when compared to BET bromodomains paralogs BRD2 and
151 BRD3[35]. Unlike the bromodomain inhibitors JQ1 and PFI1, MZ1 treatment leads to the
152 complete removal of BRD4 protein from the cell (Fig. 2d). To ensure that BRD4 was
153 completely removed from centromeres, we performed immunofluorescence for BRD4 and
154 CENP-A in HeLa cells following MZ1 treatment and confirmed the global loss of BRD4 signal,
155 including at the centromere-core (Fig. 2e and 2f).

156 To determine if BRD4 is necessary for the cohesion of centromeres we quantified cohesion
157 defects in metaphase chromosome following MZ1 treatment. We used a scale, ranging from
158 partial centromere defect to complete cohesion failure, in chromosome spreads prepared from
159 HEK293T and HeLa cells (Fig. 2g). This revealed that MZ1 treatment led to a highly
160 significant increase in centromere cohesion defects (Fig. 2h). These results identify a
161 previously uncharacterised role for BRD4 in the organisation of centromere cohesion and
162 demonstrate that PROTAC inhibitors targeting BRD4 strongly disrupt metaphase chromosome
163 architecture in different cell types (Fig. 2i).

164

165 ***JQ1 promotes the cohesion function of BRD4 at centromeres***

166 Focusing on studies exploring the effect of JQ1 on BRD4 localisation, we observed an increase
167 in centromeric BRD4 in all 15 studies we investigated (Fig. 3a), and in 25 out of 26 different
168 cell-lines within these studies (Fig. 3b). Only the JQ1-resistant cell-line SUM149R[36,37] did not
169 show an increase in centromere localised BRD4 following JQ1 treatment. JQ1 binds with lower
170 affinity to the bromodomains of BRD2 and BRD3[17], and analysis of matched ChIP-seq
171 experiments confirms BRD4 as the dominant protein recruited to centromeres upon JQ1
172 treatment (Fig. S1a). Plotting the change in BRD4 localisation between JQ1 and DMSO-treated
173 cells onto the T2T genome shows that the centromere is the principle locus gaining BRD4
174 association in different cell lines (Fig. 3c). We observed no change in BRD4 abundance
175 following JQ1 at LINE2 repeat-elements, indicating that our observations are not an artefact of
176 aligning to highly repetitive DNA (Fig. S1a and S1b). At genes and enhancer elements BRD4
177 is recruited by histone acetylation and recruits RNA polymerase II, but no increase in H3K27ac
178 or consistent changes in RNA polymerase II level were observed at centromeres following JQ1
179 treatment (Fig. 3c, Fig. S1a and S1c). Furthermore, meta-analysis of RNA-seq datasets from
180 12 studies does not identify a significant change in centromeric transcription following JQ1
181 treatment (Fig. 3d). This indicates that the JQ1-dependent recruitment of BRD4 to centromeres
182 is not linked to the proteins canonical function in transcription regulation.

183 One striking implication of our observations is that JQ1-treatment should affect centromere
184 function differently compared to PROTAC degradation of BRD4. Defects in centromeric
185 chromatin can activate cell-cycle checkpoints, leading to an accumulation of cells in G2/M, or
186 override the spindle-assembly checkpoint, promoting the transition to G1[6,38,39] (Fig. 3e). One
187 previous study directly compared cell-cycle profiles for cells treated with MZ1 and JQ1,

188 identifying that BRD4-degradation led to an accumulation of cells before mitosis whereas JQ1
189 treatment enriched for cells in G1[40]. To identify if this is a general observation across cell types
190 we consulted 94 studies with FACS data. We observed a similar trend when comparing BET-
191 degrading (e.g. dBET6) and BET inhibiting compounds (Fig. 3f, Fig. S1d). This suggests that
192 JQ1 has a distinct mechanism of action that can promote the transition of cells through mitosis.

193 To determine whether the non-canonical role for BRD4 in chromatin cohesion is affected by
194 the JQ1-dependent enrichment of BRD4 at centromeres, we quantified cohesion defects in
195 metaphase chromosome spreads prepared from JQ1-treated HEK293T and HeLa cells. In
196 contrast to PROTAC-based degradation, JQ1 treatment identified fewer centromere cohesion
197 defects (Fig. 3g). The total proportion of defects in HEK293T cells was similar between JQ1
198 and MZ1, but with a significant shift towards milder defects composed principally of the
199 'mixed' phenotype. More strikingly, in HeLa cells the proportion of cells with chromosome
200 defects is significantly lower following JQ1 treatment compared to MZ1 treatment, with levels
201 comparable to DMSO (Fig. 2h), suggesting the possibility that BRD4 recruitment stabilises
202 centromeric chromatid cohesion (Fig. 3h).

203

204 ***JQ1 is a molecular glue stabilising an interaction between BRD4 and CENP-B***

205 To identify whether JQ1 causes a total reorientation of BRD4 towards centromeric chromatin
206 we performed immunofluorescence on HeLa cells following JQ1 treatment, and observed no
207 significant change in the overall abundance of BRD4 at centromeric regions (Fig. S2a and S2b).
208 This could be explained by the fact that the observed change in centromeric BRD4 abundance
209 using ChIP-seq is subtle and yet significant, suggesting that REDPOINT has a higher
210 sensitivity to determine novel chromatin interactions than could be achieved by a microscopy-
211 based screen.

212 To investigate at the molecular scale how BRD4 is further recruited to and maintained at the
213 centromere upon JQ1 treatment we analysed published co-IP mass spectrometry (coIP-MS)
214 data identifying the proteins which specifically interact with BRD4 following JQ1
215 treatment[36,41]. In all available datasets JQ1 treatment induced a strong, and previously
216 overlooked, association between BRD4 and key centromere proteins (Fig. 4a, Fig. S2c and
217 S2d). For example, in data from SUM149 breast cancer cells, JQ1 treatment leads to a gain of
218 interaction between BRD4 and centromere-core proteins including CENP-B, CENP-C, CENP-
219 H and MIS18BP1. Across all four cell-types assayed, and in as little as 10 minutes following

220 JQ1 addition, a top new interaction was observed between BRD4 and CENP-B, a centromeric
221 protein that binds the CENP-B box sequence within α-satellite DNA[19] (Fig. 4a, Fig. S2c and
222 S2d). Members of the MIS18 complex (MIS18A, MIS18B and MIS18BP1), which binds the
223 centromere for a few minutes each anaphase to licence the deposition of CENP-A[42], were also
224 highly enriched in different coIP-MS experiments but were considered unlikely to be the major
225 factor recruiting BRD4 due to the transient interaction with centromeres.

226 CENP-B is a component of centromeric chromatin and binds constitutively to the 17bp CENP-
227 B box DNA sequence found on every centromere except the Y-chromosome[19]. Consistent with
228 a central role for CENP-B in BRD4 recruitment to the centromeres, JQ1 recruits BRD4 only
229 to α-satellite DNA and not to other centromeric DNA repeats without CENP-B boxes (Fig.
230 S3a) and to all centromeres except for the Y chromosome (4 out of 5 male cell-lines
231 investigated) (Fig. 4b, Fig. S3b). Analysis of the proportion of CENP-B CUT&RUN aligned
232 to each centromere also confirms a strong positive correlation with the enrichment of BRD4
233 following JQ1 (Fig S3c), but not with RNA polymerase II following JQ1, or BRD4 following
234 PROTAC degradation with dBET6 (Fig. S3d). Together, these observations strongly support
235 CENP-B as the key protein mediating the JQ1-dependent recruitment of BRD4 to centromeres.

236 To independently confirm that BRD4 and CENP-B interact in cells following JQ1 addition, we
237 performed coIP-western blot in HeLa and HEK293T cells (Fig. 4c, Fig. S4a). We observe a
238 strong JQ1-dependent interaction between BRD4 and CENP-B, but not between BRD4 and
239 CENP-A or CENP-C (Fig. S4b) This interaction was not observed in co-IP following treatment
240 with the (-) enantiomer of JQ1[17] or the BET bromodomain inhibitor PFI1[43], which has a
241 different chemical structure (Fig. S4c). In addition to BRD4 JQ1 has a lower affinity for the
242 other BET bromodomain proteins BRD2 and BRD3[17]. By analysing published coIP-MS of
243 these proteins we identify a weak (BRD3) or no (BRD2) JQ1-dependent interaction with
244 CENP-B (Fig. S4d), suggesting that CENP-B principally interacts with BRD4 following JQ1.

245 To identify whether the JQ1-dependent interplay between BRD4 and CENP-B is direct, we
246 reconstituted the interaction *in vitro* including biotinylated oligos containing the CENP-B box
247 DNA sequence or a 'shuffled' control version of the same sequence, purified full-length CENP-
248 B protein, purified bromodomains of BRD4 ($BRD4^{bromo)}$, and (+)-JQ1 or control (-)-JQ1
249 enantiomers (Fig. 4d). We observed that CENP-B protein is strongly associated with the
250 CENP-B box DNA sequence when compared to a shuffled version (Fig. 4 e to f). The addition
251 of (+)-JQ1 or (-)-JQ1 enantiomer to CENP-B alone did not change the level of interaction with

252 the CENP-B box, indicating that these small-molecules have no effect on CENP-B alone.
253 BRD4^{bromo} is enriched in the presence of CENP-B bound CENP-B box DNA compared to
254 shuffled DNA, even with the (-)-JQ1 enantiomer, indicating that a low-affinity complex
255 between BRD4 and CENP-B occurs independently of the BRD4-JQ1 association. However,
256 with the addition of the (+)-JQ1 enantiomer, BRD4^{bromo} and CENP-B become significantly
257 more enriched, indicating that (+)-JQ1 stabilises the BRD4-JQ1-CENP-B-DNA complex *in*
258 *vitro*. The stabilisation of a low-affinity interaction is one of the defining properties of a rare
259 class of drugs called molecular-glues, which enable gain-of-function interactions that can target
260 previously undruggable pathways[20,21], and our evidence suggests that JQ1 is the first
261 centromere-targeting drug via this mechanism-of-action.

262

263 ***The BRD4-JQ1-CENP-B complex can stabilise centromere cohesion***

264 If the BRD4-JQ1-CENP-B complex stabilises the centromere cohesion role of BRD4,
265 removing CENP-B should have centromere cohesion defects comparable to MZ1 treatment
266 (Fig. 4g). To test this hypothesis, we generated HEK293T and HeLa cells lacking CENP-B
267 through a CRISPR knock-out (CENP-B KO) approach (Fig. 4h, Fig. S5a). In HEK293T CENP-
268 B KO cells we observed a marginal enhancement of the already well-established cohesion
269 defect following JQ1 treatment (Fig. S5b). However, in HeLa CENP-B KO cells we observed
270 a massive increase in centromere cohesion defects compared to control cells, comparable to
271 the degradation of BRD4 and consistent with our proposed model (Fig. 4i). These observations
272 indicate that JQ1 has a cell-type variable role in targeting centromere structure and function,
273 through a novel complex between CENP-B and BRD4.

274 Interestingly, among the 26 different cell lines analysed in this study, only the JQ1-resistant
275 cell-line SUM149R[36,37] did not show an increase in centromere localised BRD4 following JQ1
276 treatment (Fig. 3b). SUM149R cells were selected in increasing concentrations of JQ1 and now
277 grow more rapidly in the presence of JQ1 than in DMSO[37]. To determine whether the
278 mechanism of resistance is SUM149R cells is linked to CENP-B, we analysed a published
279 CRISPR-KO screen in parental and resistant cells treat with DMSO or JQ1[36]. CENP-B is a
280 non-essential protein in SUM149 (wild-type) cells treated with DMSO or JQ1 because knock-
281 out does not significantly alter cellular proliferation, consistent with published observations
282 including viable CENP-B KO mice[44]. In contrast, SUM149R (JQ1 resistant) cells are highly
283 sensitive to the loss of CENP-B protein (Fig. 4j). In rapidly growing SUM149R-JQ1 cells,

284 CENP-B KO reduces cell proliferation, whereas in slowly growing SUM149R-DMSO cells,
285 CENP-B KO gives the most significant increase in cell proliferation out of 18,461 proteins
286 tested. We identify no other protein with a similar response amongst BET bromodomain
287 proteins, transcription elongation components, cohesin complex components or components of
288 centromeric chromatin (Fig. S5c). These observations suggest that CENP-B specifically
289 regulates cell proliferation in a model of JQ1 resistance and indicates that the BRD4-JQ1-
290 CENP-B complex is critical in establishing JQ1 resistance.

291

292 **Discussion**

293 In this study, we utilised human ChIP-seq samples to identify novel centromere proteins and
294 the BET bromodomain inhibitor JQ1 as the first drug that directly targets centromere chromatin
295 composition. A molecular-glue mechanism-of-action enables JQ1 to stabilises a direct protein-
296 protein interaction between BRD4 and the centromere DNA binding protein CENP-B. The
297 identification of molecular-glues is rare, but each new example opens up the possibility of
298 targeting previously undruggable pathways[20,21]. Future optimisation of JQ1 structure could
299 form the basis of a new class of centromere drugs targeting chromosome segregation, a process
300 which is important only in dividing cells. We show that the BRD4-JQ1-CENP-B interaction
301 stabilises centromere cohesion in mitosis, supporting a direct role for BRD4 in centromere
302 cohesion. This result complements recent findings in the interphase genome, where BRD4 has
303 been shown to regulate the structure of TADs by acting upstream of cohesin loading[25,34].

304 One of the significant challenges in employing current BET bromodomain inhibitors for cancer
305 treatment is the swift emergence of resistance[45,46]. We observed, in a preclinical model of JQ1-
306 resistance, a shift in the functional importance of CENP-B from being non-essential in JQ1-
307 sensitive cells to becoming the most significant determinant of cell proliferation in JQ1-
308 resistance cells. This finding underscores the need for future advances in bromodomain
309 inhibitors intended for clinical use to account for the centromere-linked role of JQ1 and BRD4,
310 to better target cancer-cell pathways and avoid mechanisms of resistance linked to CENP-B.

311

312

Acknowledgements

We would like to acknowledge the bwForCluster Helix and MLS&WISO for computational infrastructure and support. We would like to thank Iain Cheeseman, Andrea Mussachio and Christopher Playfoot for critical feedback on the manuscript, and Daniele Fachinetti, Aubry Miller and the Erhardt lab for valuable comments, discussions and reagents.

We acknowledge support by the Deutsche Forschungsgemeinschaft (DFG) through the grant EXC81 (CellNetworks) and GRK2039, and the European Research Council (ERC) through the grant ERC-CoG-682496 (cenRNA) to SE. NB was supported by a DKFZ postdoctoral fellowship and the ERC through the grant agreement n°805338. Computational infrastructure was supported by the state of Baden-Württemberg through bwHPC and the DFG through grants INST 35/1597-1 FUGG and INST 35/1134-1FUGG. AMS and VD are members of the graduate school HBIGS.

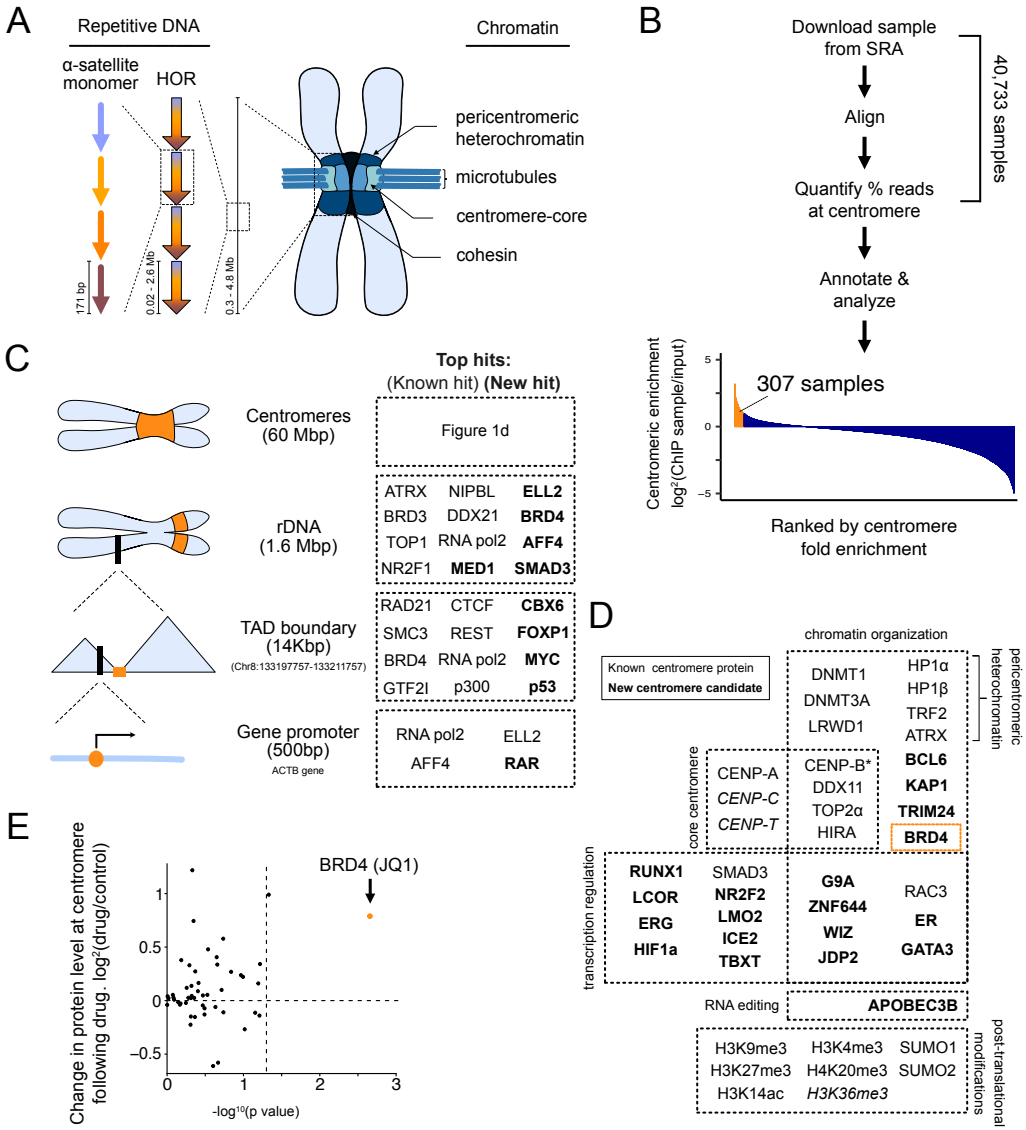

Fig. 1. BRD4 is a centromere protein which is further enriched by the bromodomain inhibitor JQ1. A) Overview of human centromeric DNA organisation and the subdomains of centromeric chromatin displayed on metaphase chromosomes. Length of DNA repeat motifs given in base-pairs (bp) and Megabases (Mb) B) Summary of the REDPOINT workflow for centromeric loci. C) REDPOINT identifies proteins associated with chromatin loci ranging from 500bp to 60Mbp in size. The top 12 proteins enriched compared to their corresponding input at rDNA and a single TAD boundary on chromosome 8 are presented, with bold proteins being novel factors. At the 500bp region of the ACTB promoter the top 4 candidates are shown. D) REDPOINT identifies 35 high confidence centromere proteins including known and novel

350 candidates. Protein categories were determined from published data and Uniprot information.
351 *CENP-B was identified using the same pipeline to analyse a published CUT&RUN dataset
352 PRJNA546288. E) Focused analysis of 50 different protein-drug pairs investigated in multiple
353 studies and identified through the REDPOINT approach. The x-axis is the statistical
354 significance from a paired-sample t-test comparing drug treatment to control across multiple
355 studies, with the vertical dotted line signifying a p-value of 0.05. The y-axis is the fold-change
356 in protein abundance at the centromere following drug treatment, with a positive fold change
357 indicating more protein at the centromere and a negative fold change indicating less protein at
358 the centromere.

359

360

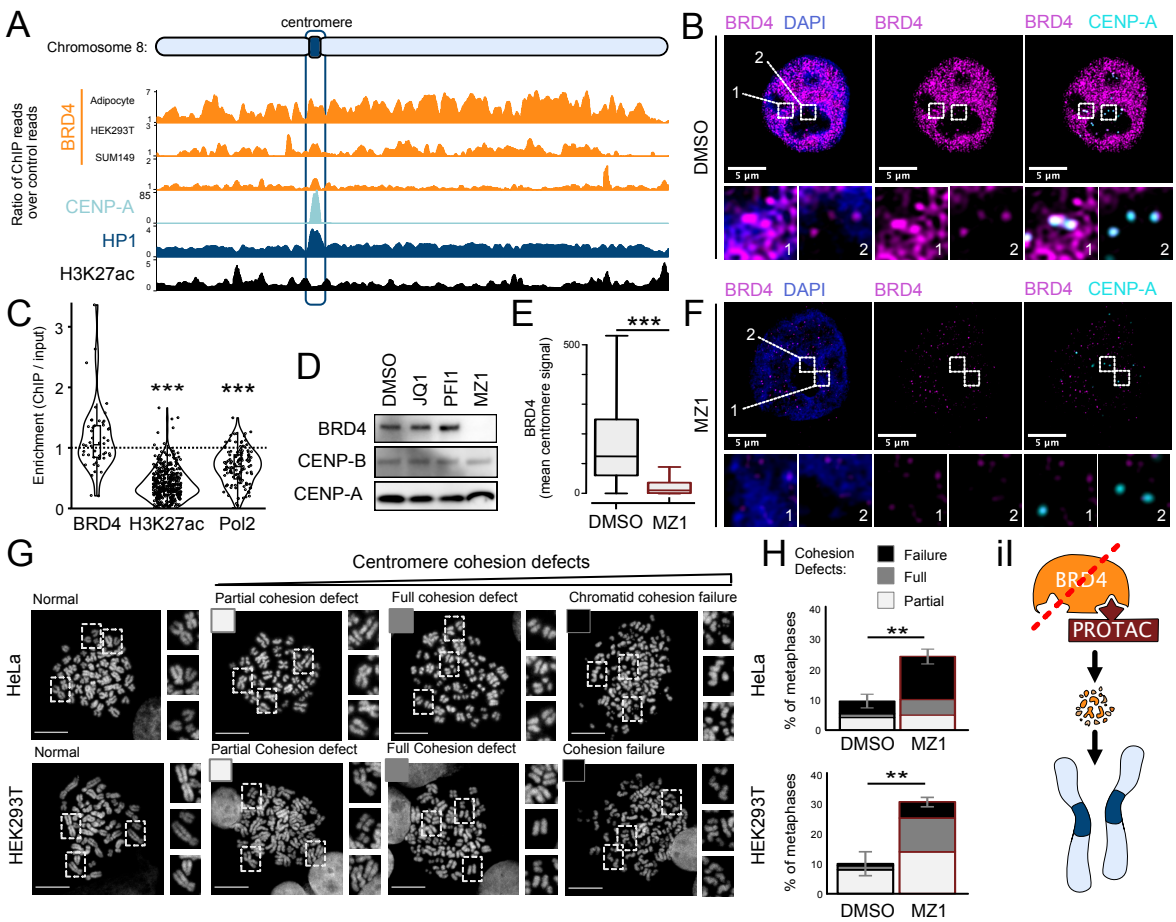

361

362 **Fig. 2. BRD4 degradation disrupts mitotic centromere cohesion.** A) Telomere-to-telomere
363 distribution of BRD4, CENP-A, HP1 and H3K27ac on chromosome 8. Data represents the ratio
364 of ChIP reads compared to a matched input from the same study. Datasets: CENP-A (HeLa)
365 PRJNA183936, BRD4 and HP1 (HEK293) PRJNA171165, H3K27ac and BRD4 (SUM149)
366 PRJNA268319, BRD4 (adipocyte) PRJNA270506. B) Immunofluorescence imaging of BRD4
367 (magenta) and CENP-A (cyan) in HeLa cells treat for 24 hours with DMSO. C) Centromere
368 enrichment of all BRD4, H3K27ac and RNA polymerase II (Pol2) ChIP-seq samples in the
369 REDPOINT dataset compared to the corresponding control from the same study. Statistical
370 analysis t-test between BRD4 and H3K27ac/Pol2 (*** $p<0.001$). D) Western blot analysis of
371 BRD4, CENP-A and CENP-B following 24 hours treatment with two bromodomain inhibitors
372 (JQ1 and PFI1) and the BRD4-specific PROTAC MZ1. E) Quantification of BRD4 signal
373 intensity at the core-centromere in HeLa cells following 24 hours DMSO or MZ1 treatment.

374 BRD4 signal intensity overlapping CENP-A foci. DMSO (n=3707 centromeres), MZ1
375 (n=3505 centromeres). Statistical analysis t-test (*** $p<0.001$). F) Immunofluorescence
376 imaging of BRD4 (magenta) and CENP-A (cyan) in HeLa cells treat following 24 hours MZ1
377 treatment. G) Representative mitotic chromosomes from HeLa and HEK293T cells with
378 normal morphology and increasing severity of centromere cohesion defect. Key for subsequent
379 quantifications in inset boxes. H) Quantification of mitotic chromosome defects following 24
380 hours MZ1 treatment in HEK293T and HeLa cells. Statistical analysis based on triplicate
381 experiments, t-test (** $p < 0.01$) i) Model outlining the effect of BRD4 degradation on mitotic
382 chromosome structure.

383

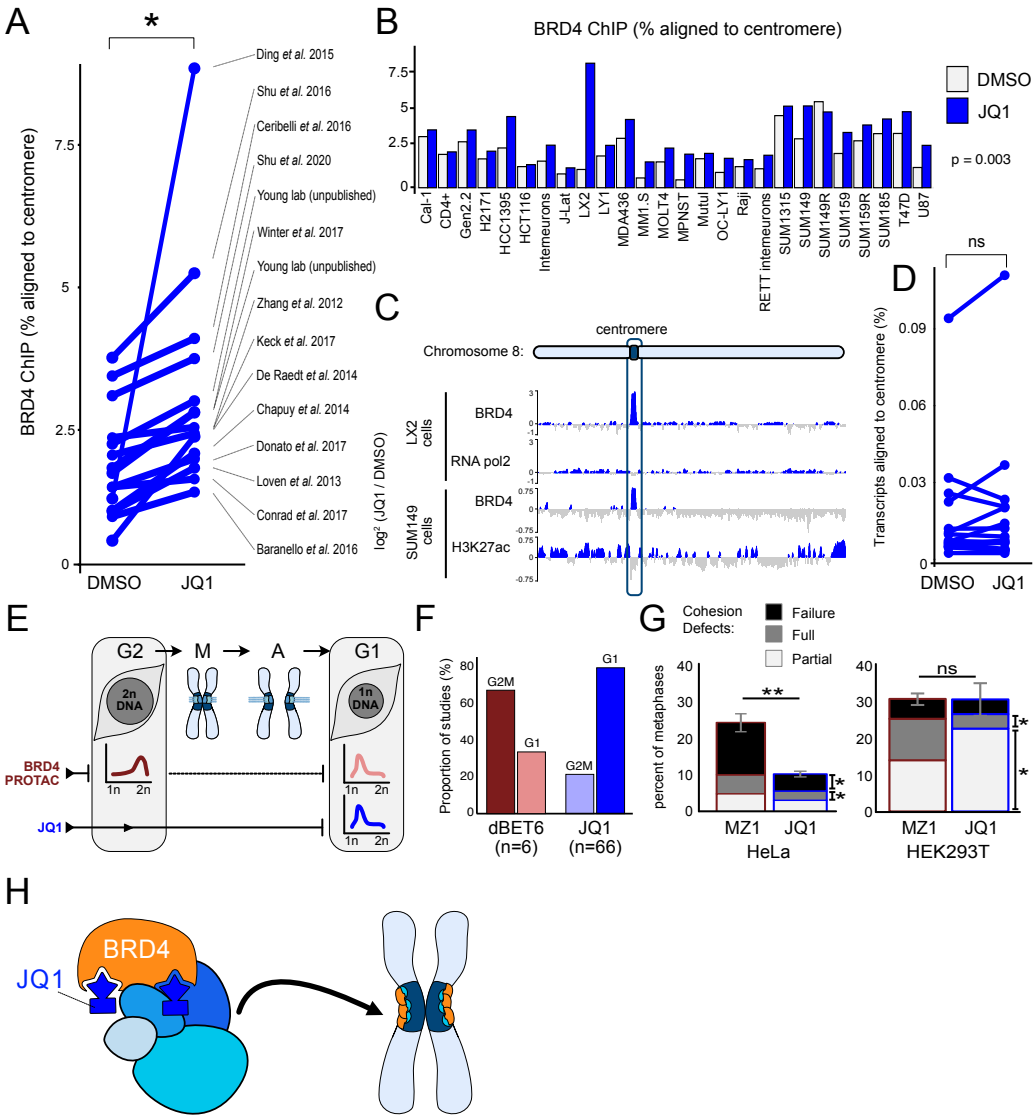

Fig. 3. JQ1 promotes a non-canonical cohesin function of BRD4 at centromeres A) Analysis of 15 different ChIP-seq datasets from studies comparing BRD4 distribution in control and JQ1 treated cells. Paired t-test p value < 0.05. B) BRD4 is more enriched following JQ1 treatment in 25 out of 26 analysed cell lines. Statistical analysis paired-sample t-test (p=0.003). C) BRD4, RNA polymerase II and H3K27ac enrichment following JQ1 compared to DMSO treatment aligned to the T2T genome of chromosome 8. LX2 data from PRJNA253142, SUM149 data from PRJNA542646. D) Meta-analysis of RNA-seq datasets comparing DMSO and JQ1 treatment from 12 studies. E) Model outlining the predicted cell-cycle profile following treatment with BRD4 degrading compounds or JQ1. F) Meta-analysis

394 of cell cycle profiling following treatment with the BRD4 PROTAC dBET6 or JQ1 taken from
395 FACS data derived from 72 published studies. Complete data for these and other
396 inhibitors/degraders from 94 studies in Supplementary Table 20. G) Quantification of mitotic
397 chromosome defects following 24 hours MZ1 or JQ1 treatment in control HEK293T and HeLa
398 cells. Key as outlined in Fig. 2G. Statistical analysis based on triplicate experiments, t-test (ns
399 'not significant', * $p<0.05$, ** $p<0.01$) H) Model outlining the rescue of centromere cohesion
400 defects in JQ1 treated cells that recruit BRD4 to the centromere.

401

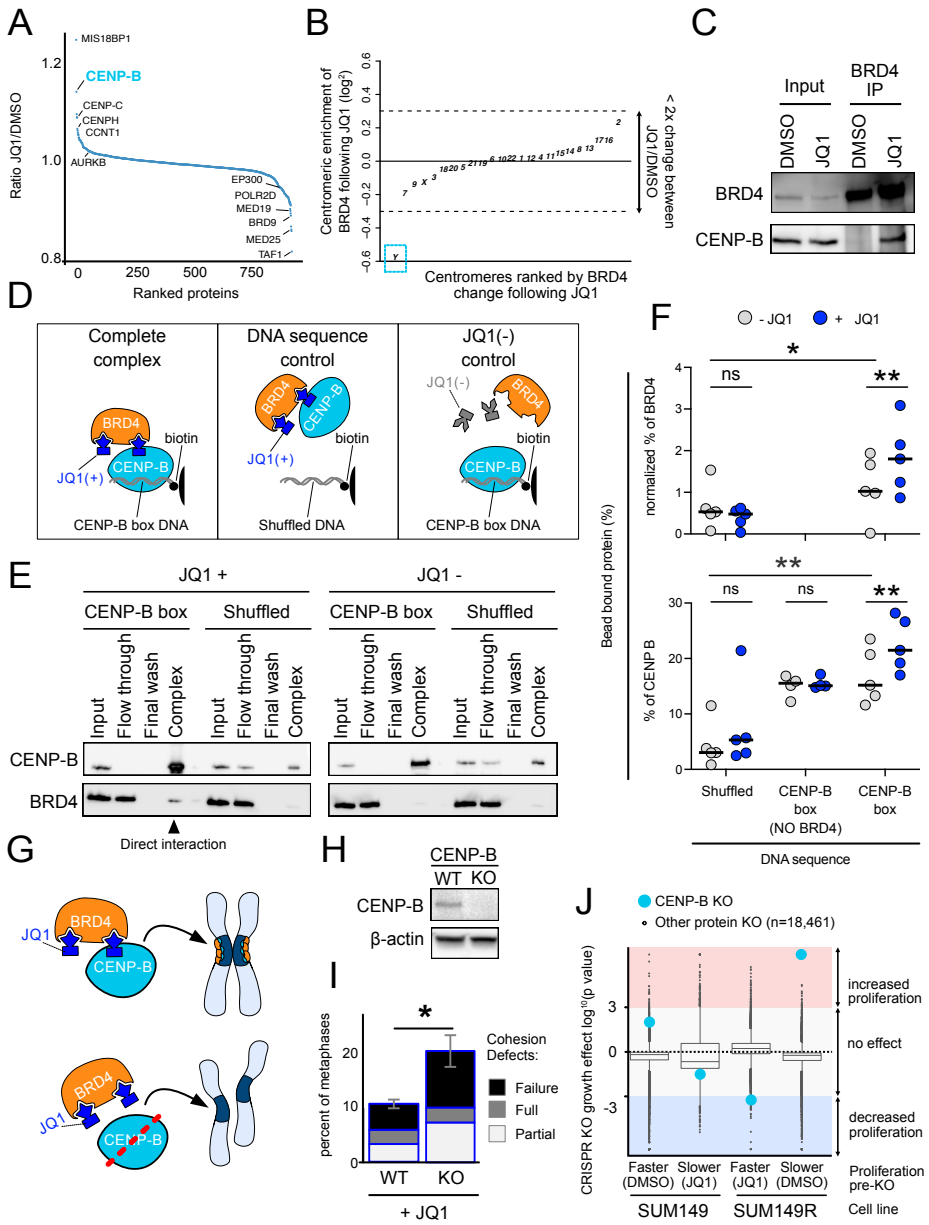

402

403 **Fig. 4. JQ1 is a molecular glue that retains BRD4 at centromeres through CENP-B.** A)
404 Co-IP MS identifying the change in proteins interacting with BRD4 following JQ1 treatment,
405 with key proteins for centromere identity and BRD4-mediated transcription regulation
406 highlighted. Data from Shu et al. (2020). B) ChIP-seq analysis of centromeres ranked by BRD4
407 enrichment following JQ1 treatment in male cells. Enrichment was calculated by identifying
408 the percentage of centromeric BRD4 at each chromosome in a sample, and then calculating the
409 ratio of JQ1 treated sample compared to DMSO treated sample. The dotted lines indicate a 2x

410 change in the abundance of a BRD4 at a centromere, the blue square highlights the Y
411 chromosome. Data from: PRJNA253142. C) Co-IP for BRD4 following DMSO or JQ1
412 treatment for 1 hour in HeLa cells, followed by western blot for BRD4 and CENP-B. D) Model
413 outlining an *in vitro* reconstitution pull-down experiment to determine whether a direct
414 interaction occurs between $BRD4^{bromo}$, (+)JQ1 and CENP-B, with control experiments
415 containing (-)JQ1 or shuffled DNA sequence. E) Example *in vitro* reconstitution pull-down
416 experiment result comprised of western blots of BRD4 and CENP-B. BRD4 is at 10x molar
417 excess compared to CENP-B. 'Input' is 10% of the total sample and 'flow through'/'wash' is
418 10% of the total. 'complex' is 100% of the bead bound protein. F) Quantification of
419 independent *in vitro* reconstitution pull-down experiments. The tenfold molar excess of BRD4
420 means that for every BRD4-CENP-B dimer there will be 9 unbound BRD4 molecules. To
421 account for this the 'Bead bound protein (% input)' for BRD4 was multiplied by ten to give
422 the 'Normalized bead bound protein (%)'. Statistical tests are paired-sample t-test (* $p<0.05$,
423 ** $p<0.01$). G) Model outlining the predicted outcome of CENP-B loss on JQ1-linked
424 centromere cohesion. H) Western blot of control (WT) and CENP-B KO HeLa cells probed
425 with anti-CENP-B antibodies and β-actin a loading control. I) Quantification of cohesion
426 defects in 24 hours JQ1-treated HeLa control and CENP-B KO cells. Statistical analysis based
427 on triplicate experiments t-test (* $p<0.05$). J) CRISPR KO screen comparing the effect of
428 CENP-B KO relative to 18,460 other proteins on cellular proliferation in JQ1-sensitive and -
429 resistance SUM149 breast cancer cells. Data from Shu et al. (2020).

430

431

432

433

434

435

436 **Materials and methods**

437 ***Candidate identification with REDPOINT***

438 *Dataset curation for analysis by REDPOINT*

439 A list of human ChIP-seq accession numbers, which allow dataset recovery from the Sequence
440 Read Archive (SRA)[14], were obtained using the 'advanced search' feature of the European
441 Nucleotide Archive (ENA) (https://www.ebi.ac.uk/ena/browser/advanced-search) with the
442 search parameters: Data type = 'Raw reads', Taxon name = 'Homo sapiens', Library Strategy
443 = 'ChIP-seq', and the field parameters: 'experiment accession' and 'sample accession'. The
444 'sample accession' enabled each dataset to be downloaded from the SRA, and the 'experiment
445 accession' allowed the samples from the same study to be grouped in downstream analyses.
446 The state of sample annotation within the SRA, ENA or the Gene Expression Omnibus (GEO)
447 did not allow for automated annotation of key features for our study, including whether the
448 sample was from a ChIP-seq experiment or corresponding input/control, the protein enriched
449 by the ChIP-seq experiment, the tissue/cell-line investigated, whether the sample was treated
450 with a drug or other experimental perturbation, and the associated PubMed ID. To enable
451 detailed downstream analysis of protein enrichment relative to corresponding input/control, the
452 influence of cell/tissue type, and the effect of perturbations including drug treatment, the first
453 21,462 samples from 1,234 studies were annotated by hand using the relevant parameters
454 included with the samples GEO submission.

455

456 *Genomic positions investigated by REDPOINT*

457 We used the hg38 genome build, which contains the entire human genome including
458 representative maps of repetitive regions[1]. We performed REDPOINT on rDNA and
459 centromeres, and at non-repetitive loci including active gene promoters identified by analysis
460 of data from the FANTOM5 consortium[47] and Topological Associated Domain (TAD)
461 boundaries previously identified at kilobase resolution[48].

462 *Detailed description of centromeric loci*

463 Centromeric repeats, are annotated in the hg38 genome and in recently published T2T
464 genomes[1,8,30]. In hg38 centromeric DNA is divided into different classes of satellite repeat,
465 including the dominant α-satellite repeat found at the centromere on every chromosome and

466 low abundance satellite classes which are each found at a small number of centromeres (GSAT,
467 GSATII, GSATX, HSAT4, SST1). The CENP-A-containing core centromere has only been
468 shown to form on the dominant α-satellite DNA[8]. α-satellite is highly divergent and has
469 different Higher Order Repeats (HORs) on different chromosomes[8]. In hg38 the centromeric
470 α-satellite repeats are sub-divided into different chromosomes based on the abundance of
471 different HORs, which allows the chromosome-specific abundance of centromeric proteins to
472 be determined from ChIP-seq data and demonstrates the detailed nature of the centromeric
473 annotation in this genome build. Recently, telomere-to-telomere (T2T) builds of the human
474 genome, with the centromeric sequence in the correct linear order across the entire domain for
475 an individual pseudo-haploid genome, have been published[8,30]. Between cell-
476 lines/chromosomes/individuals there is a strong divergence in the position and abundance of
477 different α-satellite HORs, as well as different epi-allele positioning of key centromere proteins
478 including CENP-A within the α-satellite DNA, and mapping short-read ChIP-seq data from a
479 diversity of sources to the complete T2T genome provides little extra positional information
480 compared to the hg38 genome. We therefore identified candidate proteins using the hg38
481 genome, some of which we validate by aligning to a T2T genome.

482

483 *REDPOINT analysis*

484 The REDPOINT pipeline utilises standard bioinformatic tools for data acquisition, genome
485 alignment and genomic position investigation. Briefly, 1.) For each sample, as determined by
486 the SRA 'sample accession', we downloaded a sub-set of 100,000 reads using 'fastq-dump'
487 from NCBI SRA Tools (parallel-fastq-dump -sra-id SAMPLE_ID --threads 4 --outdir out/ --
488 split -3 --gzip). The -3 split argument automatically differentiates between single-end and
489 paired-end sequencing. For consistency across the analysis, and because our analysis focuses
490 on highly repetitive DNA, we only utilised the first read of paired-end sequencing in
491 downstream analysis. We selected reads starting at read 10,000 to avoid observed problems at
492 the start of a file and obtain a random assortment of reads
493 (https://edwards.flinders.edu.au/fastq-dump/). In all cases where we compared a sample sub-
494 set aligned to the complete sequencing run we observed an exact correspondence in the
495 percentage of reads at the centromere, indicating that 100,000 reads are sufficient to identify
496 protein enrichment for a locus comprising 2.15% of the genome without generating sampling
497 bias. 2) We used Bowtie2[49] (ver.2.3.0) to align reads to the hg38 build of the human genome

498 using default settings. 3) We identified the percentage of reads at each genomic position (e.g.
499 centromeric loci, ACTB gene promoter, etc.) using HTseq[50]. This information was recorded
500 and then the loop re-set to begin the next ChIP-seq dataset.

501

502 *Quality control of ranked protein enriched at different loci*

503 The first method utilised for identifying the proteins associated with different loci of interest
504 was to rank samples based on the percentage of ChIP-seq reads associated with each locus.
505 This allowed the use of the full 40,734 samples analysed in the REDPOINT approach and
506 identified well characterised proteins associated with centromeric chromatin, rDNA, TAD
507 boundaries and gene promoter regions. We also noted many examples of artefact proteins
508 enriched via this approach. For example, there were samples which were very highly enriched
509 at centromeric loci, comparable to key CENP proteins, but upon further inspection showed no
510 enrichment compared to control samples within the same study – indicative of a problem with
511 the entire study rather than a new centromeric protein. This suggested to us that the 'ranked
512 data' approach was sufficient to identify candidate proteins, but could be improved upon by
513 comparing samples to corresponding input/control. For smaller loci including the 500bp
514 surrounding promoters we were only able to focus on the ranked data because fold-enrichment
515 is not possible when only analysing 100,000 reads per sample. Using this subset for a 500bp
516 locus identifies enriched ChIP-seq samples but gives insufficient coverage for input or control
517 samples. Investigation of 500bp regions using fold-change over corresponding input would
518 necessitate at least 10 million reads analysed per sample, but was not the focus of this study
519 and the ranked analysis of gene promoters was sufficient for a proof-of-principle.

520 *Quality control of fold-enriched proteins at different loci*

521 The second method for identifying the proteins associated with different loci of interest had a
522 number of quality control steps which take advantage of the 21,462 annotated ChIP-seq
523 samples. Input and control samples provided an invaluable quality control metric, firstly to
524 exclude problematic datasets and secondly to benchmark the proportion of centromeric DNA
525 identified in the samples within a study, which varied by around four-fold from around 1% to
526 around 4% for the majority of samples. Analysis of genomic DNA samples in the same cell
527 line across multiple studies suggested that these differences reflects inter-study variability,
528 rather than biological variability, which may be linked to differential PCR efficiency of highly
529 repetitive loci or variability in the loss of highly compact centromeric chromatin dependent on

530 the methodology used for genomic DNA or control preparation[51]. Many studies did not include
531 a genomic input sample, IgG pull-down or other corresponding control and we excluded these,
532 retaining 11,881 samples from 887 studies. Focussing on the genomic DNA or control samples
533 in these studies, we noted that a sub-set of these samples contained virtually no DNA which
534 aligned to centromeric loci. This is not biologically possible and suggests a technical problem
535 with these samples, which may reflect experimental issues or mistakes in data handling. For
536 example, it is conceivable that some samples were aligned to an older genome build and then
537 converted back into a file format that was uploaded as the 'raw data' when in fact it was
538 partially processed in a manner that lost centromeric reads. We removed all studies with fewer
539 than 1% of the reads aligned to centromeric DNA which left us with 9,764 samples from 780
540 studies, i.e. 63% of the annotated studies. For each of these samples we calculated the fold-
541 enrichment for each ChIP-seq sample compared to the inputs or controls in the same cell type
542 from within the same study. This data was then ranked for each locus of interest from most
543 enriched protein to least enriched protein.

544 We first looked at the most enriched proteins for each locus (with the exception of gene
545 promoters as discussed above). Focussing on rDNA, a single TAD boundary on chromosome
546 8 and the centromere we performed a number of quality control checks based on technical and
547 biological expectations. We looked at all of the samples within a study containing an enriched
548 protein, as we observed that problematic samples were often contained within problematic
549 studies. In most cases there was no reason for concern, but examples where enriched-proteins
550 would be excluded include studies with unusually low input/control samples which gave
551 spurious enrichment to all samples in the study, including for proteins which are consistently
552 not enriched in other studies. We also looked at instances of a 'top hit protein' in other studies,
553 and noted whether the protein had previously been observed at the locus in published
554 manuscripts or whether the protein was a new candidate locus-specific protein. We identified
555 the most robust top-hit proteins by focussing on examples that were strongly supported within
556 single studies (i.e. enriched compared to other proteins assayed) and/or across multiple studies.

557

558 ***REDPOINT validation using published datasets***

559 The BioProject accession number (PRJNA######) for each relevant study is included in the
560 figure legend.

561 *Confirming the centromere localisation of top-hit proteins identified by REDPOINT*

562 To confirm the localisation of the top-hit centromere proteins we repeated the analysis using
563 the complete sequencing run. Each ChIP-seq sample was downloaded using 'fastq-dump' from
564 NCBI SRA Tools or directly from the SRA Explorer website (https://sra-explorer.info/). The
565 technical quality of each sample was assessed using FastQC. Each sample was then aligned to
566 the hg38 version of the human genome using Bowtie2 (ver.2.3.0), converted to .bam file using
567 samtools (ver.1.3.1) and to .bed file using BEDTools (ver.2.26). Aligned files were intersected
568 with a custom table of repetitive regions extracted from the hg38 genome build, or with a table
569 of unique sequence regions including gene promoters and TAD boundaries, using the
570 'intersect' function in BEDTools. The total number of aligned reads and the proportion aligned
571 to different repetitive regions, including centromeres, was calculated using custom bash scripts
572 and processed for visualisation in R using ggplot2.

573

574 *Visualising BRD4 as a centromere protein on a T2T genome*

575 To plot BRD4 and other centromere proteins across a complete chromosome we utilised the
576 recently published T2T genome build of human chromosome 8[30]. We followed the same
577 mapping strategy as outlined in the T2T publication[30], which utilises samtools (ver.1.3.1) and
578 the alignment package bwa (ver.0.7.17)[52] with the following parameters (bwa mem -k 50 -c
579 100000 PATH/CHM13.chr8.fasta FILE.fastq > FILE.sam). To convert .sam files to .bam we
580 used samtools sort with the following parameters (samtools sort FILE.sam -o FILE.bam) and
581 samtools index (samtools index FILE.bam). To plot the genomic distribution of BRD4 or other
582 centromeric proteins compared to corresponding input we utilised the bamCompare function
583 in BEDTools (ver.2.30.0) with the following parameters (bamCompare -b1 SAMPLE.bam -b2
584 INPUT.bam --scaleFactorsMethod SES --operation ratio --binSize 1000 --samFlagExclude
585 2308 --outFileFormat bedgraph -o NAME.bedGraph). The bedGraph files were uploaded to
586 the UCSC genome browser (https://genome.ucsc.edu/) and the 'mean' signal visualised with
587 smoothing set to 10.

588

589 *Identification and validation of JQ1-dependent increase in centromeric BRD4*

590 To validate BRD4-JQ1 as the most prominent hit we included additional ChIP-seq datasets
591 investigating BRD4 following JQ1 treatment which were missed in our annotated REDPOINT
592 data, giving a total of 15 analysed datasets. We followed the same approach outlined above to

593 confirm the centromere localisation using the hg38 and T2T genome. To visualise the fold
594 change in BRD4 localisation following JQ1 treatment on the T2T genome we utilised the
595 bamCompare function in BEDTools (ver.2.30.0) with the following parameters (bamCompare
596 -b1 JQ1_sample.bam -b2 DMSO_sample.bam --scaleFactorsMethod SES --operation log2 --
597 binSize 1000 --samFlagExclude 2308 --outFileFormat bedgraph -o NAME.bedGraph). The
598 bedGraph files were uploaded to the UCSC genome browser (https://genome.ucsc.edu/) and
599 the 'mean' signal visualised with smoothing set to 5. To further characterise the effect of JQ1
600 treatment on centromeric H3K27ac, RNA polymerase II and transcription we analysed ChIP-
601 seq and RNA-seq datasets using the same approaches.

602

603 *Chromosome specificity of BRD4 centromere recruitment by JQ1*

604 We analysed the enrichment of BRD4 following JQ1 at different annotated repeats within the
605 centromere to identify evidence for a central role of CENP-B in recruiting BRD4. We first set
606 out to determine if α-satellite DNA, which is the only centromeric satellite that contains the
607 CENP-B box DNA sequence, is the most enriched repeat class. To do this we aligned matched
608 BRD4-JQ1 and BRD4-DMSO samples to the hg38 genome build, intersected with the custom
609 table of repetitive regions, and quantified the percentage of reads aligned to each class of
610 centromeric repeat. Next, we used the same data to focus on the chromosome-specific
611 breakdown of centromeric repeats that recruit BRD4 following JQ1 treatment. We calculated
612 the percentage of centromeric reads aligned to the centromere of each chromosome in each
613 sample. We then determined the ratio of JQ1 compared to DMSO for each centromere in
614 matched JQ1/DMSO pairs to focus on the relative change in BRD4-association across
615 centromeres, independent of centromere length or changes in the total level of BRD4 across all
616 centromeres. Finally, we compared the relative abundance of CENP-B on each centromere to
617 the enrichment of BRD4 following JQ1, using published CENP-B CUT&RUN and BRD4
618 ChIP-seq data. Enriched chromosomes contain more BRD4 and/or CENP-B than would be
619 expected based on the size of the centromere. The CENP-B data was generated in HeLa, a
620 female cell-line, therefore we cannot assay the Y-chromosome. As negative controls, we
621 compared centromeric CENP-B enrichment to RNA polymerase II JQ1/DMSO treatment and
622 BRD4 following degradation of BRD4 with a PROTAC inhibitor (dBET6/DMSO).

623

624 *Immunoprecipitation mass spectrometry analysis*

625 Processed BRD4 co-immunoprecipitation mass spectrometry (coIP-MS) data was obtained
626 from the supplementary information of two articles[36,41]. For SUM149/R cells the ratio of JQ1
627 to DMSO was calculated from the peptide level in the 'RIME filtered list' in Supplementary
628 Table S3, and our observations are consistent with data presented in Figure 1E of this study[36].
629 Data from HEK293T and K562 cells were calculated from Supplementary Table S2G and S2H
630 based on the fold-enrichment of each protein in the pull-down vs control[41]. The ratio of the
631 JQ1 enrichment over the DMSO enrichment was used to identify the proteins most enriched
632 upon JQ1 treatment. Co-IP MS data from this study was also analysed for BRD2 and BRD3
633 to determine the specificity of the identified drug-dependent protein complexes.

634

635 *Analysis of published FACS data*

636 More than 1800 publications identified in PubMed with the search term 'BRD4' were screened
637 for studies that identified the cell-cycle distribution of drug-treated cells using FACS analysis,
638 identifying 94 relevant studies. In each of these studies we identified from the text which
639 inhibitor or siRNA treatment used and the associated cell-cycle defect observed.

640

641 *Analysis of published CRISPR KO screen in SUM149/R cells*

642 Processed CRISPR KO screen data for SUM149 and JQ1-resistant SUM149R cells in the
643 presence DMSO or JQ1 were obtained from the Supplementary Information of a recent
644 resource article[36]. This data contained the p-values for the enrichment of each protein-targeting
645 sgRNA compared to control sgRNAs. Enriched sgRNAs have a positive value and highlight
646 proteins that are toxic in the cell-line/drug-treatment, and those that are depleted have negative
647 values and are essential for cell proliferation in the cell-line/drug-treatment. Our analysis is
648 broadly similar to Figure 1a in the source publication[36], and uses the same cut-off of $p>0.001$
649 for candidate hits but focused on pathways which were not considered or highlighted in the
650 original publication, including proteins involved in centromere function, the spindle assembly
651 checkpoint and sister chromatid cohesion

652

653 *Producing Figures*

654 All data processing and presentation in boxplots, bar charts, line graphs and other forms of
655 graphical and statistical analysis was performed in R using standard tools and ggplot2. All
656 immunofluorescence, metaphase spread and western blot images were processed in ImageJ by
657 changing the brightness/contrast only. All figures were assembled in Affinity Designer.

658

659 ***Experimental procedures used in validation of REDPOINT results***

660 *Cell Culture*

661 Human cell lines HEK293T originally obtained from the American Type Culture Collection
662 (ATCC) and HeLa SNAP CENPA (referred to throughout as HeLa cells) were obtained from
663 the Fachinetti lab (Institut Curie). Cells were cultured in DMEM (Gibco #61965-026)
664 supplemented with 10% Foetal Bovine Serum (Capricorn scientific FBS-12A), 1%
665 penicillin/streptomycin (Capricorn scientific PS-B) and sodium pyruvate at a final
666 concentration of 1mM.

667

668 *Bromodomain inhibitor treatment*

669 HEK293T and HeLa cells were treated with 0.25% DMSO (Sigma D8418) or bromodomain
670 inhibitors dissolved in DMSO to give a final concentration of 0.25% DMSO plus inhibitor.
671 Cells were treated for 1 hour or 24 hours, stated in the figure legends, with 500nM JQ1 (Sigma
672 SML0974), 500nM JQ1 (+) or (-) enantiomers (Millipore 500586) or 5μM PFI1 (Torris 4445),
673 a bromodomain inhibitor with a distinct structure and mechanism of action to JQ1 that requires
674 10x higher concentration for the same reduction in cell growth[43]. In addition, BRD4
675 degradation was achieved by 24 hours incubation with the PROTAC Inhibitor 500nM MZ1
676 (provided by Boehringer Ingelheim opnMe portal).

677

678 *Immunofluorescence*

679 HEK293T or HeLa cells were seeded on coverslips in 6-well plates and incubated at least
680 overnight to enable cells to settle and grow on the surface. Cover slips were washed gently
681 once in PBS followed by 7 minutes fixation in 4% PFA, 3x 5-minutes wash in PBS,

682 permeabilization in 0.3% Triton X-100 for 7 minutes and 3x 5-minutes PBS wash. Fixed cells
683 were blocked in 1% BSA in PBS for 30 minutes at room temperature before overnight
684 incubation at 4°C in primary antibodies: α-mouse CENP-A (1:1000 Abcam ab13939
685 (discontinued) or 1:1500 Enzo ADI-KAM-CC006-E) and α-rabbit BRD4 (1:900 Abcam
686 ab128874). The following day fixed cells were washed 3x 10-minutes in PBS and then
687 incubated 1 hour in secondary antibodies (Alexa Fluor 488, 546 or 647) before 3x 10-minute
688 wash in PBS, 5 minutes incubation in DAPI solution to stain the DNA, 1x PBS wash and mount
689 slide/coverslip with Aqua Poly Mount (Polysciences Inc. 18606-20). Imaging was performed
690 on a Zeiss AiryScan2 LSM900 confocal microscope using the 'airyscan mode' and following
691 standard operating procedures[53].

692

693 *BRD4 co-IP*

694 HEK293T or HeLa cells were split into 1x 10cm dish per IP and allowed to grow overnight
695 before treatment with DMSO, 500nM JQ1 or 5μM PFI1 for 1 hour. We utilised the Active
696 Motif Nuclear Complex Co-IP kit (#54001) following the manufacturer's instructions with the
697 following variations: we incubated the 'enzyme shearing cocktail' for 2 minutes at 37°C, we
698 used the 'gentle IP buffer' to wash samples. The immunoprecipitation antibody was α-rabbit
699 BRD4 (Bethyl A301-985-A-M).

700

701 *Western blot analysis*

702 Standard western blot procedures were followed for the quantification of protein abundance in
703 a variety of samples including following BRD4 co-IP. Briefly protein samples were prepared
704 from experimental samples or cell pellets by resuspending in 1x final concentration Laemmli
705 solution, followed by water bath sonication (Diagenode Bioruptor Plus) to reduce sample
706 viscosity and a 5-minute incubation at 95°C to ensure complete protein denaturation. Samples
707 were loaded on a 4-15% gradient gel (Bio-Rad 4561083) and run at 150v for 1 hour (Bio-Rad
708 system). The protein was transferred to PVDF membrane (Amersham 10600022) using semi-
709 dry transfer apparatus using the 'mixed MW' setting (Bio-Rad trans blot turbo). Membranes
710 were blocked for 1 hour in 5% powdered milk in TBS-T, followed by overnight primary
711 antibody incubation at 4°C. Primary antibodies used: α-mouse CENP-A (1:1000 Abcam
712 ab13939 (discontinued) or 1:1500 Enzo ADI-KAM-CC006-E), α-rabbit CENP-B (1:500

713 Abcam ab25734), α-rabbit CENP-C (1:50 Abcam ab193661), β-actin (Sigma A3854) and α-
714 rabbit BRD4 (1:500 Bethyl A301-985-A-M). Following overnight incubation membranes were
715 washed 3x 10-minutes in TBS-T, then incubated in α-mouse-HRP (Sigma A9044) or α-rabbit-
716 HRP (Sigma A0545) in 5% milk for 1 hour at room temperature. Membranes were then washed
717 3x 10-minutes in TBS-T followed by a brief incubation in ECL reagent. Chemiluminescence
718 was detected using chemiluminescent substrate (Thermo 34095 or 34575).

719

720 *Generating CENP-B CRISPR KO cell lines*

721 CRISPR KO cell lines and matched 'safe guide' controls were generated in HEK293T and
722 HeLa cells using lentivirus-mediated gene KO. HEK293T cells were also used to produce the
723 lentivirus. The first step towards generating CENP-B KO cell lines was to establish CAS9
724 stable cell lines for HEK293T and HeLa cells. Cell lines were transduced with lentiCas9-
725 Blast[54] (Addgene, #52962) and selected with 20 μg/ml blasticidin to generate stable CAS9-
726 expressing cell lines. sgRNA for CRISPR KO were designed using the Sanjana lab tool
727 (http://guides.sanjanalab .org/) and cloned as previously described[5,16]. Briefly, sgRNAs were
728 cloned by annealing two DNA oligos and ligating into a BsmB1-digested pLKO1-puro-U6-
729 sgRNA-eGFP. This construct was transformed into Stbl3 bacteria. For virus production 1
730 million HEK293T cells were transfected with 3 μg of the pLKO1-puro-U6-sgRNA-eGFP
731 plasmid and two helper vectors (2.5 μg psPAX2 and 0.9 μg VSV-G). Packaging cells were
732 transfected using polyethyleneimine (Polysciences, 23966-2) by mixing with DNA in a 3:1
733 ratio. 48 hours post-transfection viral supernatants were collected, filtered through a 0.45 μm
734 filter and supplemented with 4 μg /ml of polybrene (Sigma) before adding to target cells.
735 Downstream experiments using sgRNA KO were performed on the pool after at least 10 days,
736 or on single-cell clones that were isolated from the pool.

737

738 *Quantifying centromere cohesion defects on metaphase spreads*

739 Metaphase spreads were prepared using a standard method for karyotype analysis using
740 Carnoy's fixative and dropping the sample onto a microscope slide[56]. This process produces
741 high resolution metaphase chromosome features, but under these fixation conditions
742 centromeric antibodies do not detect their epitope[57], which prevents fluorescence microscopy.
743 Briefly, 1 well of a 6-well plate per sample was seeded two days prior to metaphase

744 chromosome preparation. 24 hours prior to metaphase chromosome preparation cells were
745 treated with DMSO or BET bromodomain inhibitors (JQ1, MZ1). 2 hours prior to metaphase
746 chromosome preparation cells were treated with 1μg/ml colcemid. Cells were then harvested,
747 combining the media, wash and cells into a single 15ml Falcon tube. To swell cells were
748 resuspended in 5ml 75mM KCl for 10-minutes at room temperature. Cells were pelleted by
749 centrifugation and resuspended in 10ml Carnoy's fixative (3-parts methanol to 1-part acetic
750 acid) and incubated for 10 minutes at room temperature. This pelleting, resuspending and
751 incubation was repeated twice more and samples were then placed at -20°C at least over-night,
752 and maintained at -20°C for long term storage. To prepare slides of metaphase chromosomes,
753 samples were recovered from -20°C storage, cells pelleted by centrifugation, resuspended in
754 10ml room temperature Carnoy's fixative, incubated for 10 minutes at room temperature,
755 pelleted and resuspended in a small amount of Carnoy's fixative dependent on the pellet size.
756 To make chromosome spreads we took 20 μL of the sample, hydrated the surface of a positively
757 charged microscope slide (Hecht 42409110) with a gentle open-mouthed blow, and quickly
758 dropped the sample from a height of approximately 10 cm. Slides were allowed to dry overnight
759 in a dark drawer. The following day slides were rehydrated for 5 minutes in PBS, incubated in
760 DAPI and mounted using Aqua Poly Mount. Imaging was performed on a Zeiss AiryScan2
761 LSM900 confocal microscope using the 'airyscan mode' and following standard operating
762 procedures. Metaphase imaging and analysis was performed blind and the categorisation of
763 centromere defects was based on published observations[58]

764

765 *In vitro reconstitution of the BRD4-JQ1-CENP-B-DNA interaction*

766 Purified BRD4^{bromo} and CENP-B, together with JQ1 enantiomers, were incubated with
767 biotinylated dsDNA made by annealing oligos containing a CENP-B box motif (F primer –
768 GGCCTTCGTTGGAAACGGGATTT) or a shuffled version of the same sequence as a
769 negative control for CENP-B binding (F primer – GTTAGCGATTTGAATTCCGGGGC) with
770 the biotin moiety linked to the 5' end of the forward primer. Full-length purified CENP-B was
771 purchased from Active Motif (No. 81201) and JQ1 (+) or (-) enantiomers were purchased from
772 Sigma (SML1524 & SML1525).

773 Sumo tagged BRD4^{bromo} (44-460 aa) was expressed in BL21 *E. coli* after induction with IPTG
774 overnight at 15°C and purified using an ÄKTA pure first with a nickel column (Cytivia HisTrap
775 HP 17524701), followed by a buffer exchange (Cytivia HiTrap Desalting 17140801), Ulp1

776 cleavage [60] and a second round of nickel chromatography to remove the SUMO tag. Protein
777 purity was determined by Coomassie stained SDS PAGE and aliquots flash frozen in liquid
778 nitrogen.

779 To prepare the magnetic beads, 15µl Dynabeads MyOne Streptavidin T1 beads (Invitrogen
780 65601) were resuspended in 100µl Binding and Wash (BW) Buffer (5mM Tris-HCl pH7.5,
781 0.5mM EDTA, 1M NaCl). A magnetic rack was used to separate the beads and the supernatant
782 was discarded. Beads were washed 3x in BW buffer, using the rack to separate the beads and
783 discarding the supernatant each time.

784 Double stranded DNA was prepared by resuspending complementary oligonucleotides in
785 annealing buffer (5mM Tris-HCl pH6.8, 1mM EDTA, 50mM KCl, 0.01% triton X-100),
786 heating to 95°C for 5 minutes followed by cooling the samples at 1°C per minute until 4°C.
787 30pmol of dsDNA was resuspended in Binding and Wash (BW) Buffer (5mM Tris-HCl pH7.5,
788 0.5mM EDTA, 1M NaCl) to a total volume of 100µl. This DNA was added to the pre-washed
789 streptavidin beads and incubated for 30 minutes at 24°C with gentle shaking to immobilise the
790 biotinylated dsDNA on the beads. The beads were then washed one time in BW Buffer and
791 twice in Binding Buffer (20mM HEPES pH7.6, 10% glycerol, 1mM EDTA, 3mM DTT, 0.05%
792 NP40, 150mM NaCl). Following the final wash beads were resuspended in 30µl Binding
793 Buffer containing 2.5 pmol CENP-B, 25 pmol $BRD4^{bromo}$ and 50 pmol (+)-JQ1 or (-)-JQ1. An
794 Input sample 3µl (10%) aliquot was taken and frozen, the remainder of the sample was
795 incubated overnight at 4°C rotating at 20rpm. The following day Binding Buffer was added to
796 a final volume of 300µl, the tube incubated on a magnetic rack, as a Flow Through sample a
797 30µl (10%) aliquot was taken and frozen, and the remaining supernatant was discarded. The
798 beads were then washed three more times in 300µl Binding Buffer, with a 30µl (10%) aliquot
799 of the Final Wash taken and frozen. After the final wash 30µl 1x Laemmli buffer was added to
800 the beads to give the Complex sample. Each of the Input samples was made up to 30µl in
801 Binding Buffer and 10µl of 4x Laemmli buffer was added to the Input, Flow Through and Final
802 Wash samples. All of the samples were boiled at 95°C for 5 minutes, centrifuged and loaded
803 on 10% SDS PAGE gels for Western Blot. Western blot was performed as outlined previously
804 with primary antibodies to BRD4 (Abcam ab128874) and CENP-B (Abcam ab25734).

805

806

807 **References**

808 1. Miga, K. H. The Promises and Challenges of Genomic Studies of Human Centromeres.
809 *Prog. Mol. Subcell. Biol.* **56**, 285–304 (2017).
810 2. Allshire, R. C. & Karpen, G. H. Epigenetic regulation of centromeric chromatin: old dogs,
811 new tricks? *Nat. Rev. Genet.* **9**, 923–937 (2008).
812 3. Black, B. *Centromeres and kinetochores: discovering the molecular mechanisms*
813 *underlying chromosome inheritance*. (Springer, 2017).
814 4. Barra, V. & Fachinetti, D. The dark side of centromeres: types, causes and consequences
815 of structural abnormalities implicating centromeric DNA. *Nat Commun* **9**, 4340 (2018).
816 5. Jeffery, D. *et al.* CENP-A overexpression promotes distinct fates in human cells, depending
817 on p53 status. *Commun Biol* **4**, 417 (2021).
818 6. Matthews, H. K., Bertoli, C. & de Bruin, R. A. M. Cell cycle control in cancer. *Nat Rev*
819 *Mol Cell Biol* **23**, 74–88 (2022).
820 7. Cohen-Sharir, Y. *et al.* Aneuploidy renders cancer cells vulnerable to mitotic checkpoint
821 inhibition. *Nature* **590**, 486–491 (2021).
822 8. Altemose, N. *et al.* Complete genomic and epigenetic maps of human centromeres. *Science*
823 **376**, eabl4178 (2022).
824 9. Lambert, S. A. *et al.* The Human Transcription Factors. *Cell* **175**, 598–599 (2018).
825 10. Panigrahi, A. & O'Malley, B. W. Mechanisms of enhancer action: the known and the
826 unknown. *Genome Biol* **22**, 108 (2021).
827 11. Rao, S. S. P. *et al.* Cohesin Loss Eliminates All Loop Domains. *Cell* **171**, 305-320.e24
828 (2017).
829 12. Valencia, A. M. & Kadoch, C. Chromatin regulatory mechanisms and therapeutic
830 opportunities in cancer. *Nat Cell Biol* **21**, 152–161 (2019).

831 13. Mitchener, M. M. & Muir, T. W. Oncohistones: Exposing the nuances and vulnerabilities
832 of epigenetic regulation. *Mol Cell* **82**, 2925–2938 (2022).
833 14. Katz, K. *et al.* The Sequence Read Archive: a decade more of explosive growth. *Nucleic*
834 *Acids Res* **50**, D387–D390 (2022).
835 15. Altendorfer, E., Mochalova, Y. & Mayer, A. BRD4: a general regulator of transcription
836 elongation. *Transcription* **13**, 70–81 (2022).
837 16. Mirkovic, M. & Oliveira, R. A. Centromeric Cohesin: Molecular Glue and Much More.
838 *Prog Mol Subcell Biol* **56**, 485–513 (2017).
839 17. Filippakopoulos, P. *et al.* Selective inhibition of BET bromodomains. *Nature* **468**, 1067–
840 1073 (2010).
841 18. Filippakopoulos, P. & Knapp, S. Targeting bromodomains: epigenetic readers of lysine
842 acetylation. *Nat Rev Drug Discov* **13**, 337–356 (2014).
843 19. Gamba, R. & Fachinetti, D. From evolution to function: Two sides of the same CENP-B
844 coin? *Exp Cell Res* **390**, 111959 (2020).
845 20. Schreiber, S. L. The Rise of Molecular Glues. *Cell* **184**, 3–9 (2021).
846 21. Wu, H. *et al.* Molecular glues modulate protein functions by inducing protein aggregation:
847 A promising therapeutic strategy of small molecules for disease treatment. *Acta Pharm Sin*
848 *B* **12**, 3548–3566 (2022).
849 22. Kong, X. *et al. The cohesin loader NIPBL interacts with pre-ribosomal RNA and treacle*
850 *to regulate ribosomal RNA synthesis*. http://biorxiv.org/lookup/doi/10.1101/658492 (2019)
851 doi:10.1101/658492.
852 23. Abraham, K. J. *et al.* Nucleolar RNA polymerase II drives ribosome biogenesis. *Nature*
853 **585**, 298–302 (2020).

854 24. Kopp, N. D. *et al.* Functions of Gtf2i and Gtf2ird1 in the developing brain: transcription,
855 DNA binding and long-term behavioral consequences. *Hum Mol Genet* **29**, 1498–1519
856 (2020).
857 25. Linares-Saldana, R. *et al.* BRD4 orchestrates genome folding to promote neural crest
858 differentiation. *Nat Genet* **53**, 1480–1492 (2021).
859 26. Kixmoeller, K., Allu, P. K. & Black, B. E. The centromere comes into focus: from CENP-
860 A nucleosomes to kinetochore connections with the spindle. *Open Biol* **10**, 200051 (2020).
861 27. Janssen, A., Colmenares, S. U. & Karpen, G. H. Heterochromatin: Guardian of the
862 Genome. *Annu. Rev. Cell Dev. Biol.* **34**, 265–288 (2018).
863 28. Eagen, K. P. BET proteins loop and compartmentalize the 3D genome. *Nat Genet* **54**, 370–
864 371 (2022).
865 29. Hoyt, S. J. *et al.* From telomere to telomere: The transcriptional and epigenetic state of
866 human repeat elements. *Science* **376**, eabk3112 (2022).
867 30. Logsdon, G. A. *et al.* The structure, function and evolution of a complete human
868 chromosome 8. *Nature* **593**, 101–107 (2021).
869 31. Sabari, B. R. *et al.* Coactivator condensation at super-enhancers links phase separation and
870 gene control. *Science* **361**, eaar3958 (2018).
871 32. Sullivan, B. A. & Karpen, G. H. Centromeric chromatin exhibits a histone modification
872 pattern that is distinct from both euchromatin and heterochromatin. *Nat. Struct. Mol. Biol.*
873 **11**, 1076–1083 (2004).
874 33. Olley, G. *et al.* Publisher Correction: BRD4 interacts with NIPBL and BRD4 is mutated in
875 a Cornelia de Lange-like syndrome. *Nat Genet* **51**, 1192 (2019).
876 34. Xie, L. *et al.* BRD2 compartmentalizes the accessible genome. *Nat Genet* **54**, 481–491
877 (2022).

878 35. Zengerle, M., Chan, K.-H. & Ciulli, A. Selective Small Molecule Induced Degradation of
879 the BET Bromodomain Protein BRD4. *ACS Chem Biol* **10**, 1770–1777 (2015).
880 36. Shu, S. *et al.* Synthetic Lethal and Resistance Interactions with BET Bromodomain
881 Inhibitors in Triple-Negative Breast Cancer. *Mol Cell* **78**, 1096-1113.e8 (2020).
882 37. Shu, S. *et al.* Response and resistance to BET bromodomain inhibitors in triple-negative
883 breast cancer. *Nature* **529**, 413–417 (2016).
884 38. Lara-Gonzalez, P., Pines, J. & Desai, A. Spindle assembly checkpoint activation and
885 silencing at kinetochores. *Semin Cell Dev Biol* **117**, 86–98 (2021).
886 39. Silva, R. D. *et al.* Absence of the Spindle Assembly Checkpoint Restores Mitotic Fidelity
887 upon Loss of Sister Chromatid Cohesion. *Curr Biol* **28**, 2837-2844.e3 (2018).
888 40. Noblejas-López, M. D. M. *et al.* Activity of BET-proteolysis targeting chimeric
889 (PROTAC) compounds in triple negative breast cancer. *J Exp Clin Cancer Res* **38**, 383
890 (2019).
891 41. Lambert, J.-P. *et al.* Interactome Rewiring Following Pharmacological Targeting of BET
892 Bromodomains. *Mol Cell* **73**, 621-638.e17 (2019).
893 42. Fujita, Y. *et al.* Priming of centromere for CENP-A recruitment by human hMis18alpha,
894 hMis18beta, and M18BP1. *Dev Cell* **12**, 17–30 (2007).
895 43. Picaud, S. *et al.* PFI-1, a highly selective protein interaction inhibitor, targeting BET
896 Bromodomains. *Cancer Res* **73**, 3336–3346 (2013).
897 44. Hudson, D. F. *et al.* Centromere protein B null mice are mitotically and meiotically normal
898 but have lower body and testis weights. *J Cell Biol* **141**, 309–319 (1998).
899 45. Trojer, P. Targeting BET Bromodomains in Cancer. *Annu. Rev. Cancer Biol.* **6**, 313–336
900 (2022).
901 46. Shorstova, T., Foulkes, W. D. & Witcher, M. Achieving clinical success with BET
902 inhibitors as anti-cancer agents. *Br J Cancer* **124**, 1478–1490 (2021).

903 47. FANTOM Consortium and the RIKEN PMI and CLST (DGT) *et al.* A promoter-level
904 mammalian expression atlas. *Nature* **507**, 462–470 (2014).
905 48. Rao, S. S. P. *et al.* A 3D map of the human genome at kilobase resolution reveals principles
906 of chromatin looping. *Cell* **159**, 1665–1680 (2014).
907 49. Langmead, B. & Salzberg, S. L. Fast gapped-read alignment with Bowtie 2. *Nat Methods*
908 **9**, 357–359 (2012).
909 50. Anders, S., Pyl, P. T. & Huber, W. HTSeq--a Python framework to work with high-
910 throughput sequencing data. *Bioinformatics* **31**, 166–169 (2015).
911 51. Henikoff, S., Henikoff, J. G., Sakai, A., Loeb, G. B. & Ahmad, K. Genome-wide profiling
912 of salt fractions maps physical properties of chromatin. *Genome Res.* **19**, 460–469 (2009).
913 52. Li, H. & Durbin, R. Fast and accurate long-read alignment with Burrows-Wheeler
914 transform. *Bioinformatics* **26**, 589–595 (2010).
915 53. Wu, X. & Hammer, J. A. ZEISS Airyscan: Optimizing Usage for Fast, Gentle, Super-
916 Resolution Imaging. *Methods Mol Biol* **2304**, 111–130 (2021).
917 54. Sanjana, N. E., Shalem, O. & Zhang, F. Improved vectors and genome-wide libraries for
918 CRISPR screening. *Nat Methods* **11**, 783–784 (2014).
919 55. Shalem, O. *et al.* Genome-scale CRISPR-Cas9 knockout screening in human cells. *Science*
920 **343**, 84–87 (2014).
921 56. Hliscs, R., Mühlig, P. & Claussen, U. The spreading of metaphases is a slow process which
922 leads to a stretching of chromosomes. *Cytogenet Cell Genet* **76**, 167–171 (1997).
923 57. Beh, T. T., MacKinnon, R. N. & Kalitsis, P. Active centromere and chromosome
924 identification in fixed cell lines. *Mol Cytogenet* **9**, 28 (2016).
925 58. Nagasaka, K. *et al.* Cohesin mediates DNA loop extrusion and sister chromatid cohesion
926 by distinct mechanisms. *bioRxiv* 2022.09.23.509019 (2022)
927 doi:10.1101/2022.09.23.509019.

928 59. Muro, Y. *et al.* Centromere protein B assembles human centromeric alpha-satellite DNA
929 at the 17-bp sequence, CENP-B box. *J Cell Biol* **116**, 585–596 (1992).
930 60. Kuo, D., Nie, M. & Courey, A. J. SUMO as a solubility tag and in vivo cleavage of SUMO
931 fusion proteins with Ulp1. *Methods Mol Biol* **1177**, 71–80 (2014).
932

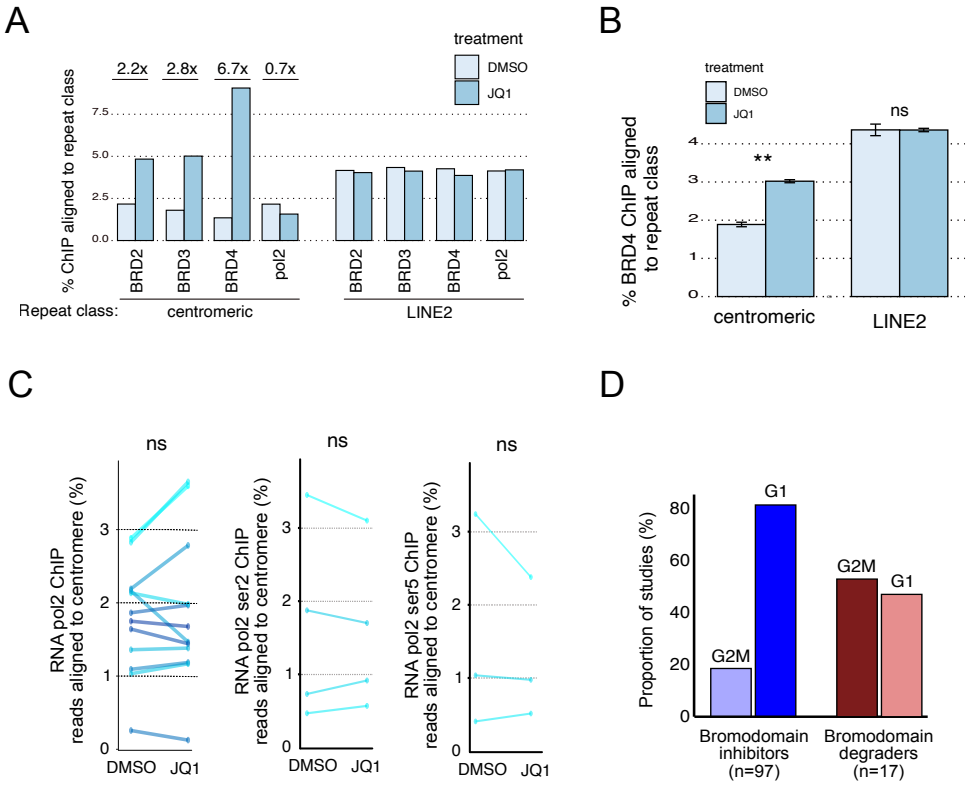

933

934 **Fig. S1. BRD4 is specifically enriched at centromeres following JQ1 treatment, but does**
935 **not recruit RNA polymerase II.** A) BRD4 is more enriched at centromeric DNA following
936 JQ1 than BRD2 or BRD3, POL2 shows no change in centromere abundance. LINE2 elements
937 show no change in the level of BRD2, BRD3, BRD4 or POL2 following JQ1. Data from:
938 PRJNA253142. B) BRD4 is significantly enriched at centromeres following JQ1 in a dataset
939 with triplicate samples, whereas BRD4 levels at LINE2 elements do not change. Data from
940 PRJNA482365. C) RNA polymerase 2 level at centromeres is not consistently affected by JQ1
941 treatment. Total pol2 – 12 studies, pol2 ser2 – 4 studies, pol2 ser5 – 3 studies. D) Meta-analysis
942 of cell cycle profiling following treatment with BRD4 inhibitor compounds or BRD4 degrading
943 compounds, taken from FACS data derived from 94 published studies.

944

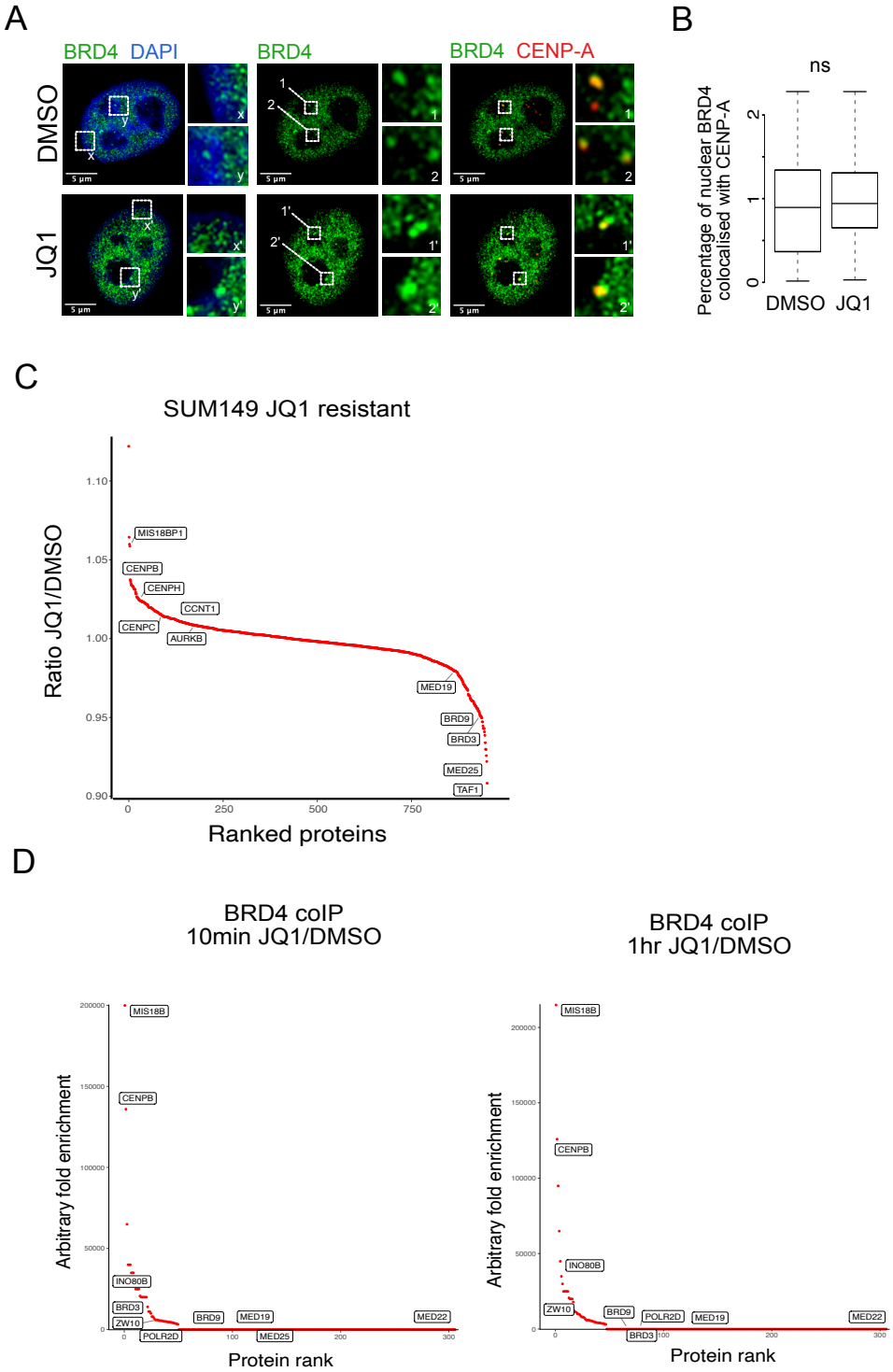
A
BRD4 DAPI
BRD4
BRD4 CENP-A
DMSO
JQ1
B
ns
Percentage of nuclear BRD4 colocalised with CENP-A
DMSO
JQ1
C
SUM149 JQ1 resistant
Ratio JQ1/DMSO
Ranked proteins
MIS18BP1
CENPB
CENPH
CCNT1
CENPC
AURKB
MED19
BRD9
BRD3
MED25
TAF1
D
BRD4 coIP
10min JQ1/DMSO
BRD4 coIP
1hr JQ1/DMSO
Arbitrary fold enrichment
Protein rank
MIS18B
CENPB
INO80B
BRD3
ZW10
POLR2D
BRD9
MED19
MED25
MED22

945

946

947

Fig. S2. JQ1 stabilises a complex containing BRD4 and centromeric proteins. A) Immunofluorescence imaging of BRD4 (green) and CENP-A (red) in HeLa cells following 24 hours DMSO or JQ1 treatment. BRD4/DAPI inset images highlight the nuclear periphery (x and x') and the nucleolar periphery (y and y'). BRD4 and BRD4/CENP-A inset images (1, 1', 2 and 2') highlight core-centromere locations (CENP-A enriched). B) Quantification of the percentage of total nuclear BRD4 signal which co-localises with CENP-A in DMSO or JQ1 treated HeLa cells. Statistical test is a t-test (n=90 cells for DMSO and 90 cells for JQ1). C) BRD4 co-IP MS in SUM149R cells comparing proteins enriched in JQ1 compared to DMSO, with key proteins for centromere identity and BRD4-mediated transcription regulation highlighted. Data from Shu et al. (2020). D) BRD4 co-IP MS in HEK293T cells comparing proteins enriched in JQ1 compared to DMSO after 10 minutes or one-hour drug treatment. Data from Lambert *et al*. 2019.

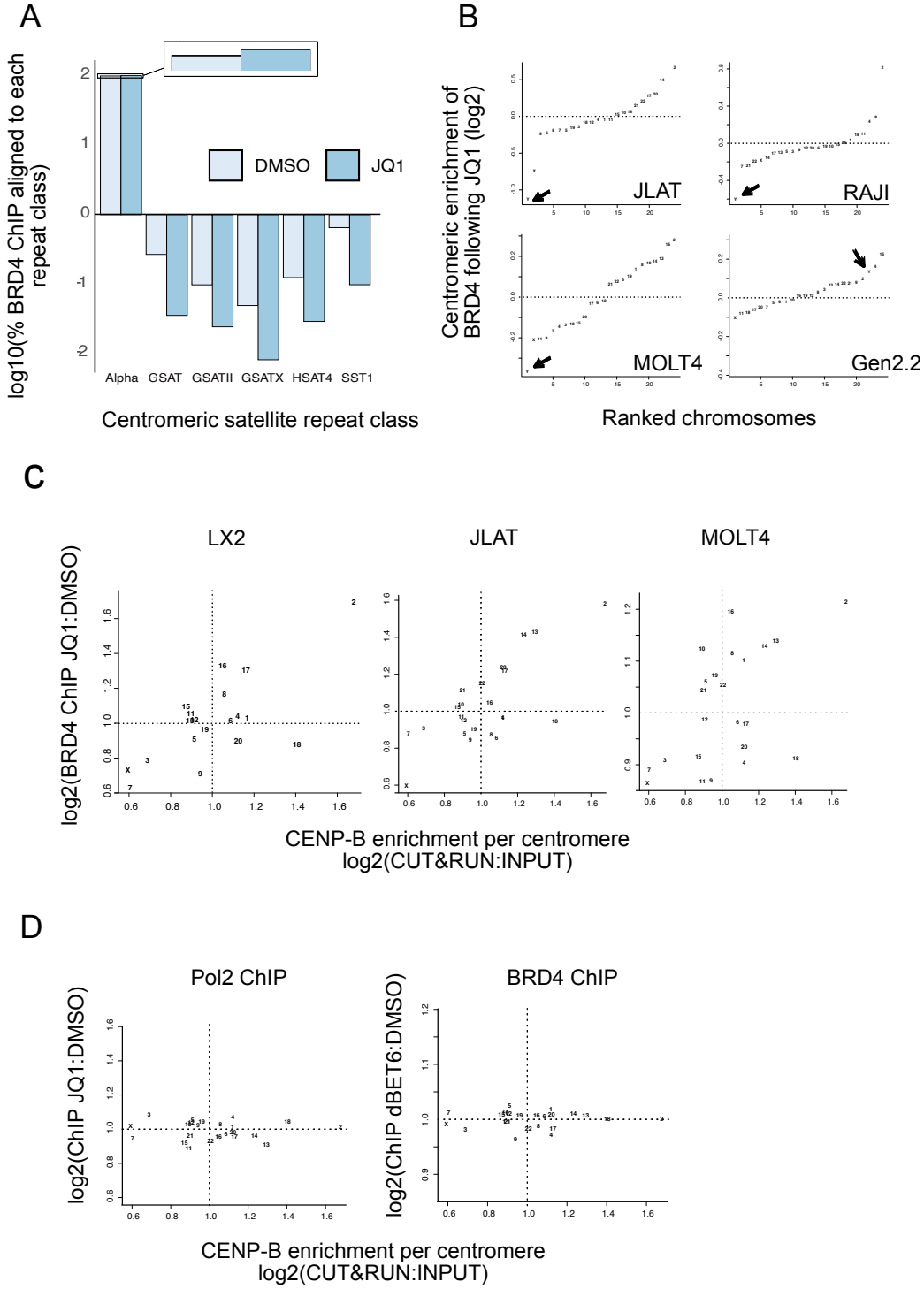
A
log10(% BRD4 ChIP aligned to each repeat class)
DMSO
JQ1
Alpha
GSAT
GSATII
GSATX
HSAT4
SST1
Centromeric satellite repeat class
B
Centromeric enrichment of BRD4 following JQ1 (log2)
JLAT
RAJI
MOLT4
Gen2.2
Ranked chromosomes
C
LX2
JLAT
MOLT4
log2(BRD4 ChIP JQ1:DMSO)
CENP-B enrichment per centromere
log2(CUT&RUN:INPUT)
D
Pol2 ChIP
BRD4 ChIP
log2(ChIP JQ1:DMSO)
log2(ChIP dBET6:DMSO)
CENP-B enrichment per centromere
log2(CUT&RUN:INPUT)

Fig. S3. BRD4 is specifically enriched at CENP-B binding sites following JQ1 treatment. A) Quantifying the percentage of reads aligning to each class of centromeric DNA repeat. Data in LX2 cells from data from PRJNA253142. B) ChIP-seq analysis of centromeres ranked by BRD4 enrichment following JQ1 treatment in male cell lines. Enrichment was calculated by identifying the percentage of centromeric BRD4 at each chromosome in a sample, and then calculating the ratio of JQ1 treated sample compared to DMSO treated sample. The arrow indicates the Y chromosome. Data: JLAT PRJNA391180, RAJI PRJNA306758, MOLT4 PRJNA315416, Gen2.2 PRJNA306431. C) Relationship between CENP-B enrichment at each centromere and BRD4 recruitment following JQ1. CENP-B CUT&RUN data from PRJNA546288, BRD4 datasets as outlined above. D) Correlation between CENP-B enrichment at each centromere and RNA polymerase II following JQ1 or BRD4 following BRD4 degradation with dBET6. Data: pol2 PRJNA253142, dBET6 PRJNA315416.

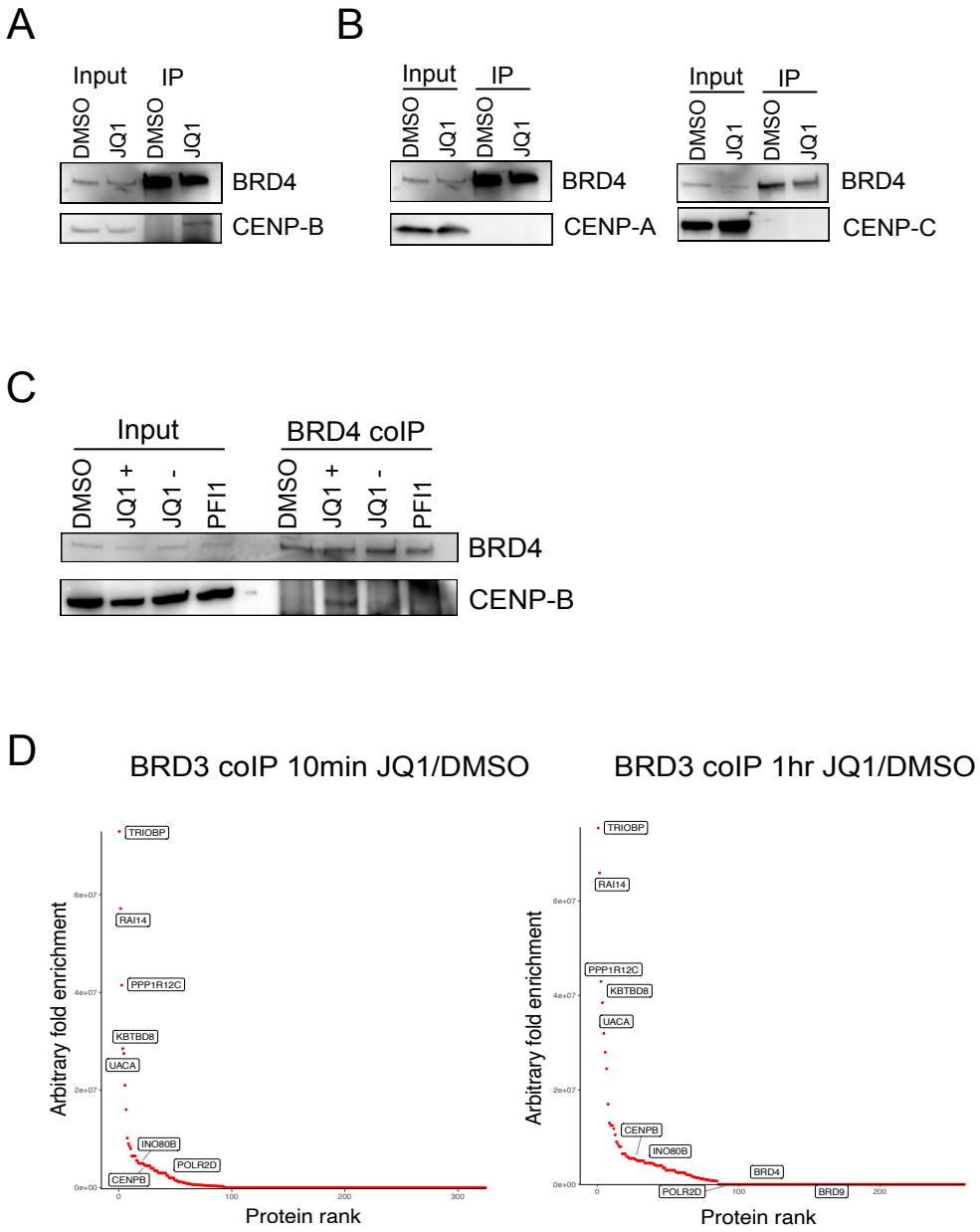

Fig. S4. A specific interaction occurs between BRD4 and CENP-B. A) Co-IP for BRD4 following DMSO or JQ1 treatment for 1 hour in HEK293T cells, followed by western blot for BRD4 and CENP-B. B) Co-IP for BRD4 following DMSO or JQ1 treatment for 1 hour in HeLa cells, followed by western blot for BRD4 and CENP-A or CENP-C. C) Co-IP for BRD4 following DMSO, (+)-JQ1, (-)-JQ1 or PFI1 treatment for 1 hour in HeLa cells, followed by western blot for BRD4 and CENP-B. D) BRD3 co-IP MS in HEK293T cells comparing proteins enriched in JQ1 compared to DMSO after 10 minutes or one-hour treatment. Data from Lambert *et al*. 2019.

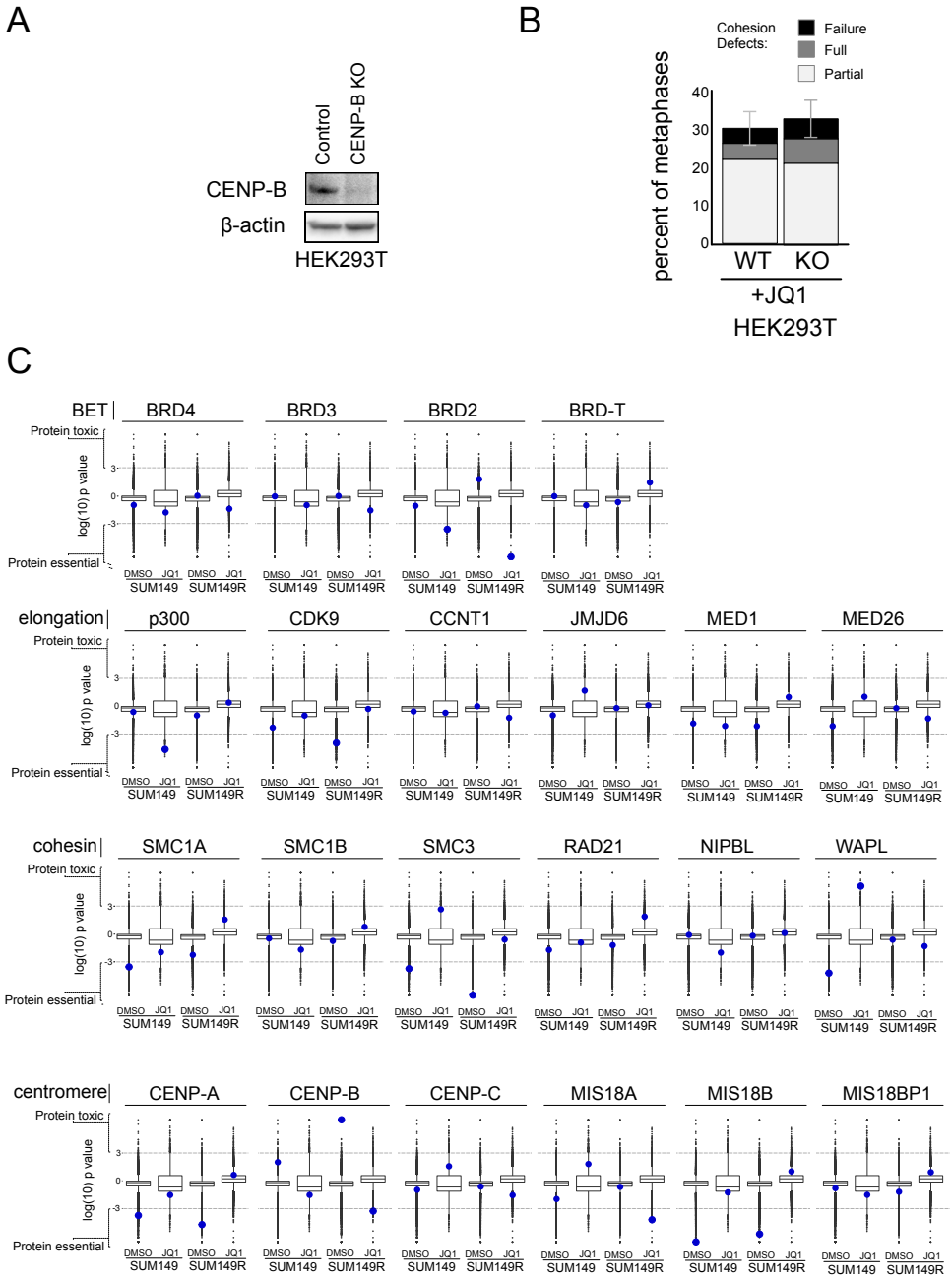

Fig. S5. CENP-B has a key role in JQ1-resistance. A) Western blot confirming CENP-B depletion in CENP-B KO in HEK293T cells. B) Quantification of cohesion defects following 24 hours JQ1 treatment in HEK293T control (WT) and CENP-B KO cells. C) CRISPR KO screen comparing the effect of different BET bromodomain proteins, transcription elongation proteins, cohesin proteins and centromeric proteins relative to 18,460 other proteins on cellular proliferation in JQ1-sensitive and -resistance SUM149 breast cancer cells. Data from Shu et al. (2020). Toxic proteins are those in which KO promotes growth, essential proteins are those where KO reduces growth.